

PL-TR-93-2228

AD-A278 569



2

**SINGLE-STATION BACKAZIMUTH ESTIMATION
FROM P- AND RG-WAVES AT REGIONAL
DISTANCE IN THE CENTRAL APPALACHIANS**

Martin C. Chapman
Shaosong Huang
J. Arthur Snoke

DTIC
ELECTE
MAR 21 1994
S F D

Virginia Polytechnic Institute
and State University
Department of Geological Sciences
Blacksburg, Virginia 24061-0420

30 November 1993

Final Report
28 March 1993 - 28 September 1993

598

94-08846



APPROVED FOR PUBLIC RELEASE; DISTRIBUTION UNLIMITED




PHILLIPS LABORATORY
Directorate of Geophysics
AIR FORCE MATERIEL COMMAND
HANSCOM AIR FORCE BASE, MA 01731-3010

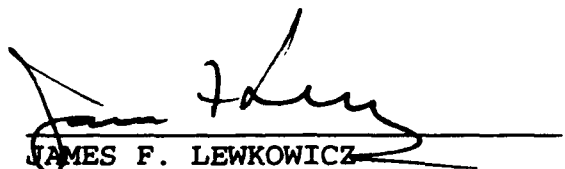
94 3 18 098

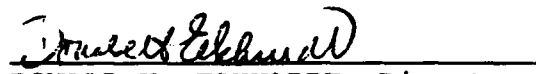
DTIC QUALITY ASSURED 1

The views and conclusions contained in this document are those of the authors and should not be interpreted as representing the official policies, either expressed or implied, of the Air Force or the U.S. Government.

This technical report has been reviewed and is approved for publication.


JAMES F. LEWKOWICZ
Contract Manager
Solid Earth Geophysics Branch
Earth Sciences Division


JAMES F. LEWKOWICZ
Branch Chief
Solid Earth Geophysics Branch
Earth Sciences Division


DONALD H. ECKHARDT, Director
Earth Sciences Division

This document has been reviewed by the ESD Public Affairs Office (PA) and is releasable to the National Technical Information Service (NTIS).

Qualified requestors may obtain additional copies from the Defense Technical Information Center. All others should apply to the National Technical Information Service.

If your address has changed, or if you wish to be removed from the mailing list, or if the addressee is no longer employed by your organization, please notify PL/IMA, 29 Randolph Road, Hanscom AFB MA 01731-3010. This will assist us in maintaining a current mailing list.

Do not return copies of this report unless contractual obligations or notices on a specific document require that it be returned.

REPORT DOCUMENTATION PAGE			Form Approved OMB No. 0704-0188	
Public reporting burden for this collection of information is estimated to average 1 hour per response, including the time for reviewing instructions, searching existing data sources, gathering and maintaining the data needed, and completing and reviewing the collection of information. Send comments regarding this burden estimate or any other aspect of this collection of information, including suggestions for reducing this burden, to Washington Headquarters Services, Directorate for Information Operations and Reports, 1215 Jefferson Davis Highway, Suite 1204, Arlington, VA 22202-4302, and to the Office of Management and Budget, Paperwork Reduction Project (0704-0188), Washington, DC 20503.				
1. AGENCY USE ONLY (Leave blank)		2. REPORT DATE 30 November 1993	3. REPORT TYPE AND DATES COVERED Final Report (28 March 1993-28 September 1993)	
4. TITLE AND SUBTITLE Single-Station Backazimuth Estimation from P- and Rg- Waves at Regional Distance in the Central Appalachians			5. FUNDING NUMBERS F19628-92-K-0029 PE 62714E PR 2A10 TA GM WU AB	
6. AUTHOR(S) Martin C. Chapman Shaosong Huang J. Arthur Snoke				
7. PERFORMING ORGANIZATION NAME(S) AND ADDRESS(ES) Virginia Polytechnic Institute and State University Department of Geological Sciences Blacksburg, Virginia 24061-0420			8. PERFORMING ORGANIZATION REPORT NUMBER	
9. SPONSORING/MONITORING AGENCY NAME(S) AND ADDRESS(ES) Phillips Laboratory 29 Randolph Road Hanscom AFB, Massachusetts 01731-3010 Contract Manager: James Lewkowicz/GPEH			10. SPONSORING/MONITORING AGENCY REPORT NUMBER PL-TR-93-2228	
11. SUPPLEMENTARY NOTES				
12a. DISTRIBUTION/AVAILABILITY STATEMENT Approved for public release; distribution unlimited			12b. DISTRIBUTION CODE	
13. ABSTRACT (Maximum 200 words) The study examines the accuracy of single-station backazimuth measurements from polarization analysis of near regional P- and Rg-wave arrivals. The data set consists of 37 signals from mining explosions in the distance range 100 to 300 km, recorded at station BLA, Blacksburg, Virginia. The station-source backazimuth estimates derived from the three-component station are compared with results derived from independent information, primarily from regional network epicenter locations. For P-wave signal/noise ratios in excess of 2.0, the mean backazimuth error of the single-station estimate is 6 degrees (for sources in the northwest quadrant) and the standard deviation is 21 degrees. Generally, only the initial (1 second or less) portion of the P-wave arrival is polarized in the source-station azimuth. Off-azimuth arrivals consisting of converted and scattered energy appear early in the P coda. Emergent P-wave arrivals from the delay-fired explosions, combined with steep apparent angles of incidence (averaging 22 degrees) complicate the single-station, three-component location problem. A subset of 27 signals featuring recognizable Rg arrivals was analyzed using a phase difference criterion. On average, the resulting backazimuth estimates are almost as reliable as those derived from the P-wave motion.				
14. SUBJECT TERMS Source-receiver backazimuth measurement, P-wave polarization, Rg-wave polarization			15. NUMBER OF PAGES 58	
			16. PRICE CODE	
17. SECURITY CLASSIFICATION OF REPORT Unclassified	18. SECURITY CLASSIFICATION OF THIS PAGE Unclassified	19. SECURITY CLASSIFICATION OF ABSTRACT Unclassified	20. LIMITATION OF ABSTRACT SAR	

Table of Contents

<u>Section</u>	<u>Page</u>
Summary.....	vii
1. Introduction.....	1
2. The Blacksburg Three-Component Station.....	1
2.1 Calibration.....	1
3. The Regional Network.....	2
4. Location and Characteristics of the Mining Explosions.....	2
5. Method of P-Wave Polarization Analysis.....	9
6. P-Wave Data Analysis.....	10
7. Results of the P-Wave Analysis.....	14
8. Rg-Wave Analysis.....	34
9. Method of Rg-Wave Polarization Analysis.....	34
10. Results of the Rg-Wave Analysis.....	36
11. Conclusions and Recommendations.....	42
12. References.....	43

Accession For	
NTIS CRA&I	<input checked="" type="checkbox"/>
DTIC TAB	<input type="checkbox"/>
Unannounced	<input type="checkbox"/>
Justification	
By	
Distribution /	
Availability Codes	
A1st /	Avail and/or Special

List of Illustrations

Figure	Page
1. Network stations (including three-component station BLA) are shown by circles. Crosses indicate mine locations yielding multiple explosion signals. Mines for which only a single explosion was recorded are shown by triangles.....	3
2. Confirmed mine locations and network derived location errors.....	7
3. Mine locations and network derived location error estimates.....	8
4. Time series data for Explosion #16 at the Starfire Mine in Kentucky.....	11
5. Fourier amplitude spectra of the vertical component P-wave arrival, Explosion #16 (solid line), and the pre-P-wave noise (dashed).....	12
6. Results of polarization processing for Explosion #16.....	13
7. Three-component station backazimuth error versus signal/noise ratio.....	15
8. Three-component station backazimuth error versus rectilinearity.....	15
9. Time series data for Explosions #35 at the Central Ohio Mine.....	16
10. Time series data for Explosion #20 at the Central Ohio Mine.....	16
11. Fourier amplitude spectrum, Explosion #35: Vertical component P-wave arrival (solid) and pre-P-wave noise (dashed).....	17

12.	Fourier amplitude spectrum, Explosion #20: Vertical component P-wave arrival (solid) and pre-P-wave noise (dashed).....	17
13.	Results of polarization processing for Explosion #35.....	18
14.	Results of polarization processing for Explosion #20.....	19
15.	Apparent angle of incident P-wave versus three-component signal/noise ratio.....	21
16.	Time series data for Explosion #9.....	22
17.	Fourier amplitude spectrum, Explosion #9: Vertical component P-wave arrival (solid) and pre-P-wave noise (dashed).....	23
18.	Results of polarization processing for Explosion #9.....	24
19.	Time series data for Explosion #12.....	25
20.	Fourier amplitude spectrum, Explosion #12: Vertical component P-wave arrival (solid) and pre-P-wave noise (dashed).....	26
21.	Results of polarization processing for Explosion #12.....	27
22.	Time series data for Explosion #17.....	28
23.	Fourier amplitude spectrum, Explosion #17: Vertical component P-wave arrival (solid) and pre-P-wave noise (dashed).....	29
24.	Results of polarization processing for Explosion #17.....	30
25.	Time series data for Explosion #33.....	31
26.	Fourier amplitude spectrum, Explosion #33: Vertical component P-wave arrival (solid) and pre-P-wave noise (dashed).....	32
27.	Results of polarization processing for Explosion #33.....	33

28.	Results of Rg phase analysis for Explosion #22.....	3 7
29.	Results of Rg phase analysis for Explosion #19.....	3 8
30.	Results of Rg phase analysis for Explosion #11.....	3 9
31.	Results of Rg phase analysis for Explosion #29.....	4 0
32.	Rg backazimuth error versus relative amplitude parameter.....	4 1
33.	Comparison of P and Rg phase backazimuth errors.....	4 1

Summary

The objective of this study is determination of the accuracy with which the station-source backazimuth can be determined from single station, three-component data in the case of industrial explosions at near regional distance. The single station backazimuth, derived from the polarization of the P-wave, was a parameter reported by U.S. stations during the GSETT-2 experiment. One of these stations (BLA), located at Blacksburg, Virginia, is situated to record numerous large mining explosions in the distance range 100 to 300 km. The explosions can be reliably located using arrival time data from a regional network.

A moving window polarization analysis of the explosion P-wave arrivals was performed. In a fashion similar to the procedures followed during the GSETT-2 experiment, maximum rectilinearity of motion was used as a criterion for judging the "best" backazimuth estimate from the three-component P-wave data. The resulting best estimate backazimuth is compared with that derived from the independently located mines.

The results of the comparisons show that three-component signal/noise ratios less than 2.0 can result in very unreliable backazimuths. However, for S/N ratios exceeding 2.0, the mean backazimuth error is 6 degrees with standard deviation 21 degrees. The error in the determinations does not appear to be strongly correlated with signal/noise ratios in the range 2 to 10.

Characteristics of the signals which contribute to the errors in the single-station backazimuth estimates include:

1. Very emergent initial motions from the delay-fired explosions.
2. Off-azimuth P-wave arrivals and/or converted phases arriving very early in the P-wave coda.
3. Steep apparent angles of incidence, averaging 22 degrees from vertical, which tend to reduce the signal/noise ratios on the horizontal components.

Optimum P-wave data segments for reliable source backazimuth estimates are restricted to very short time intervals (1 second or less) beginning with the initial P-wave motion.

A subset of data featuring Rg arrivals was analyzed using a phase difference criterion to estimate the station-source backazimuth. The mean backazimuth error for 27 events is -2 degrees: the standard deviation is 26 degrees, which is only 5 degrees larger than the result obtained from the P-wave arrivals. This suggests that Rg can be used to reliably estimate the source direction in some situations.

1. Introduction

As part of the GSETT-2 experiment, a high-quality six-channel (three component short-period and broadband) seismic system was installed at Blacksburg, Virginia, in January, 1990. The Blacksburg location is well situated to record industrial explosions in the distance range 100 to 300 km arising from surface coal mining operations in Ohio, West Virginia and Kentucky.

This report examines the accuracy with which the source-station backazimuth can be determined at station BLA from polarization analysis of the mining explosion generated P-wave and Rg-wave signals. As a basis for the accuracy assessment, the backazimuths derived from the three component analysis at BLA are compared with the locations of the mines estimated using arrival time data recorded at stations of the Virginia Tech and Tennessee Valley Authority regional seismic networks.

2. The Blacksburg Three-Component Station

The Blacksburg, Virginia, GSETT-2 station was installed in January, 1990 in the WWSSN vault on the campus of Virginia Tech. This vault is founded on Cambrian dolomite of the Appalachian Valley and Ridge geologic province. The station is equipped with Teledyne Geotech GS-13 short-period and BB-13 broadband sensors. Digitization, multiplexing and calibration are performed by a Teledyne-Geotech RDAS-200 unit, and time synchronization is obtained via a Kinometrics, Inc. Omega receiver/clock. The short-period and broadband sample rates are 40 and 10 samples/sec, respectively. The data are demultiplexed, event-detected and archived by a Science Horizons, Inc. NOMAD workstation.

2.1 Calibration

Relative differences in system response on the two horizontal components result in systematic errors in backazimuth estimates.

Hence, the system responses of the short-period channels were determined.

The RDAS-200 unit provides for the capability of either pulse-type transient or sinusoidal steady state calibration test signals to be applied to the sensor calibration circuits. The transient calibration pulses were used to determine the short-period system response using the approach described by Chapman et al. (1988). Essentially, the method fits an ideal damped oscillator amplitude response to the Fourier amplitude spectrum of a recorded system calibration pulse. A nonlinear least squares algorithm is used to estimate the system period, damping and gain.

The amplitude responses of the horizontal channels were found to differ by less than 2 percent in the 1 to 10 Hz frequency band. The vertical component response differs from that of the two horizontals by approximately 9 percent. These differences were removed by mathematical correction of the recorded data.

3. The Regional Network

The network stations used to determine the locations of mining explosions are shown in Figure 1. The six stations in western Virginia and in West Virginia are operated by Virginia Tech, whereas the stations in Tennessee and Kentucky are part of a network operated by the Tennessee Valley Authority (TVA). The Virginia Tech stations are recorded digitally in an event triggered mode. The TVA stations are recorded on 16 mm Develocorder photographic film.

4. Location and Characteristics of the Mining Explosions

Figure 1 shows the locations of the 37 mining explosions used in the study. Examination of the signals using trace overlays recorded by the Virginia Tech network indicates that the data set consists of multiple explosions at nine mine sites plus single explosions at nine additional sites. Confirmation of the geographic

locations of the explosions through contact with the mine operators has been achieved for three mines. These three confirmed locations are the Central Ohio Mine in southeastern Ohio, the Ruffner Mine in West Virginia and the Starfire Mine in eastern Kentucky, shown in Figure 2.

The epicenters of the explosions were located using the combined Virginia Tech and TVA network arrival time data (both P and S-Lg arrival times). The location program HYPOELLIPSE (Lahr, 1980) was used with a three layer crustal velocity model (Bollinger et al., 1980). The network locations and location quality estimates are given in Table 1. In cases where the event epicenter was not known from independent information and where multiple events were recorded from the same location, the network location with smallest statistical uncertainty was adopted as the epicenter of the group of explosions.

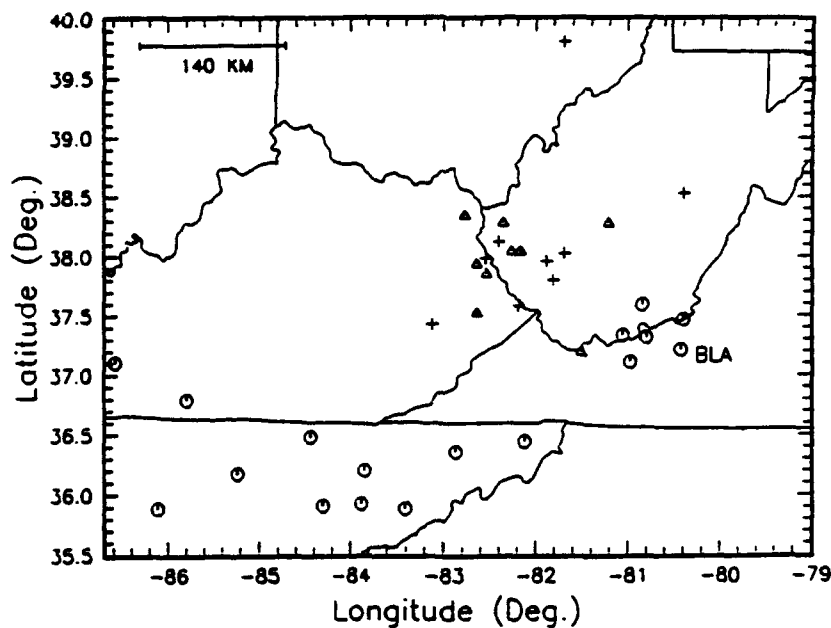


Figure 1. Network stations (including three-component station BLA) are shown by circles. Crosses indicate mine locations yielding multiple explosion signals. Mines for which only a single explosion was recorded are shown by triangles.

Table 1

EVENT NO.	Mine ¹	LAT (Deg. N)	LONG (Deg. W)	ERH ² (km)	DIST (km)	BAZ (Deg.)	BAZ (Est)	RECT	S/N
20	A	39.80	81.69	-	308	339	334	0.88	1.1
21	A	39.80	81.69	-	308	339	368	0.91	1.4
31	A	39.80	81.69	-	308	339	20	0.93	1.7
35	A	39.80	81.69	-	308	339	239	0.87	1.7
36	A	39.80	81.69	-	308	339	331	0.89	2.2
10	B	37.43	83.12	-	241	277	275	0.99	3.0
13	B	37.43	83.12	-	241	277	250	0.98	7.2
16	B	37.43	83.12	-	241	277	270	0.96	7.2
28	B	37.43	83.12	-	241	277	289	0.97	4.1
44	B	37.43	83.12	-	241	277	243	0.97	3.8
15	C	37.80	81.81	-	139	298	248	0.94	6.1
47	C	37.80	81.81	-	139	298	271	0.98	3.8
19	-	38.53	80.39	15	146	1±4.2	357	0.88	1.8
22	-	38.53	80.39	11	146	1±4.2	9	0.85	3.2
12	-	38.13	82.40	7	202	301±1.5	299	0.98	6.9
39	-	38.13	82.40	7	202	301±1.5	286	0.98	5.0
43	-	38.13	82.40	21	202	301±1.5	313	0.94	3.1
18	-	37.99	82.54	5	206	295±0.7	280	0.97	3.3
32	-	37.99	82.54	3	206	295±0.7	265	0.98	9.5
24	-	37.58	82.18	8	161	285±2.8	144	0.93	1.4
38	-	37.58	82.18	9	161	285±2.8	283	0.93	1.3
41	-	37.58	82.18	10	161	285±2.8	314	0.96	5.4

Table 1 (continued)

EVENT NO.	Mine ¹	LAT (Deg. N)	LONG (Deg. W)	ERH ² (km)	DIST (km)	BAZ (Deg.)	BAZ (Est)	RECT	S/N
17	-	38.03	81.69	9	144	309±1.6	307	0.96	4.4
42	-	38.03	81.69	9	144	309±1.6	311	0.91	2.5
34	-	38.03	81.69	5	144	309±1.6	320	0.90	2.5
27	-	37.96	81.88	14	154	303±2.1	287	0.94	3.0
33	-	37.96	81.88	7	154	303±2.1	308	0.97	8.7
8	-	38.34	82.78	17	243	302±3.6	308	0.92	2.0
9	-	37.52	82.64	99	200	280±2.3	279	0.96	4.8
11	-	38.04	82.26	11	187	300±2.2	273	0.95	3.8
14	-	37.94	82.65	6	212	293±1.1	264	0.96	6.9
25	-	37.19	81.51	12	97	269±4.5	274	0.94	3.7
26	-	37.85	82.54	7	200	292±1.7	284	0.90	3.3
29	-	38.28	82.36	4	208	305±1.0	279	0.97	7.9
37	-	38.28	81.21	6	137	330±2.2	336	0.89	2.4
40	-	38.04	82.16	19	179	304±3.7	252	0.97	3.2

¹A = Central Ohio Coal Company;

B = "Starfire" Mine, eastern Kentucky;

C = "Ruffner" Mine, Arch Minerals, Inc., Yolyn, West Virginia;

- = Mine location derived from network arrival time data: not confirmed by independent information

²ERH = Horizontal error measure from location program HYPOELLIPSE.

³Errors estimated on the basis of the angles subtended by the HYPOELLIPSE 68% confidence error ellipses.

The location capabilities of the network were examined by comparing the network derived epicenter locations of the Starfire, Ruffner and Central Ohio Mines with their known locations. Figure 2 shows the HYPOELLIPSE 68% chi-square confidence regions for the horizontal projections of the hypocenter locations. Also shown in the figure are the actual locations of the three mines. The network locations for the explosions at the Starfire Mine in Kentucky and the explosions at the Ruffner Mine in West Virginia are in good agreement with the actual locations. The network location capability for the Ohio explosions is degraded because of very low signal-to-noise ratios for that more distant source.

Figure 3 shows the location error ellipses for the remaining events in the data set. With the exception of Event 9 in Kentucky, which was well recorded only by the Virginia Tech network, the error ellipse semi-major axes are all less than 25 km. The uncertainty in the network derived backazimuths must be taken into consideration in order to assess the quality of the single-station estimates. The horizontal angles subtended by the HYPOELLIPSE error ellipses as viewed from station BLA were calculated and are listed in Table 1. The maximum uncertainty, as defined by the angular extent of the error ellipse, is ± 4.6 degrees, for Event #25. This error estimate does not account for any systematic bias due to inaccuracy of the velocity model. However, this latter source of error appears to be small, for as shown in Figure 2, the calculated locations of the Starfire and Ruffner Mines are near the true mine locations.

Information obtained from the mine operators at the three mines indicates that the larger explosions usually are the result of "cast blasting," a technique which typically utilizes delay-fired, multi-row charge designs, similar to the explosions studied by Chapman et al. (1992).

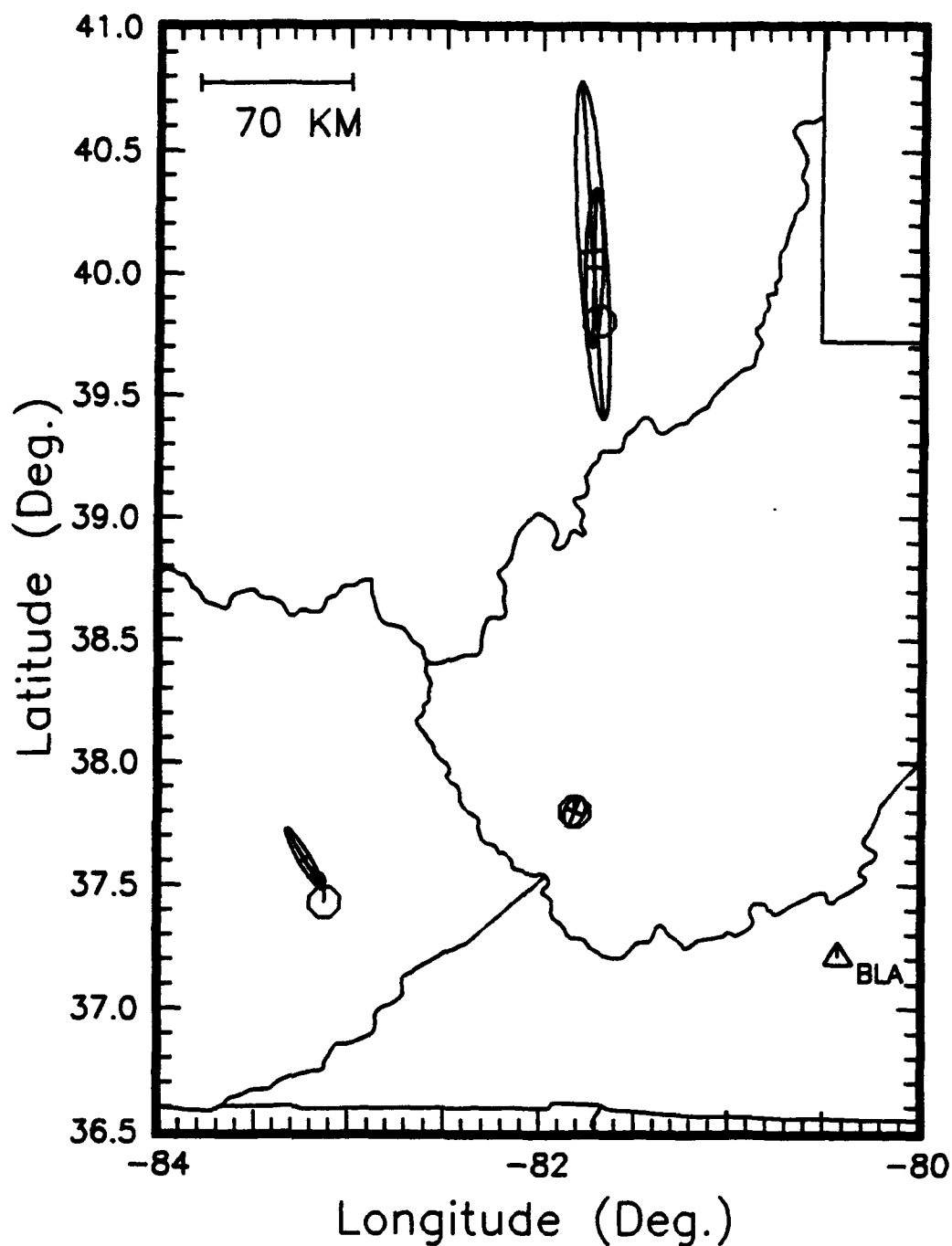


Figure 2. Confirmed mine locations are shown by the circles. Location of station BLA shown by the triangle. Ellipses indicate the horizontal projections of the 68% chi-square confidence ellipsoids for blast epicenters from location program HYPOELLIPSE.

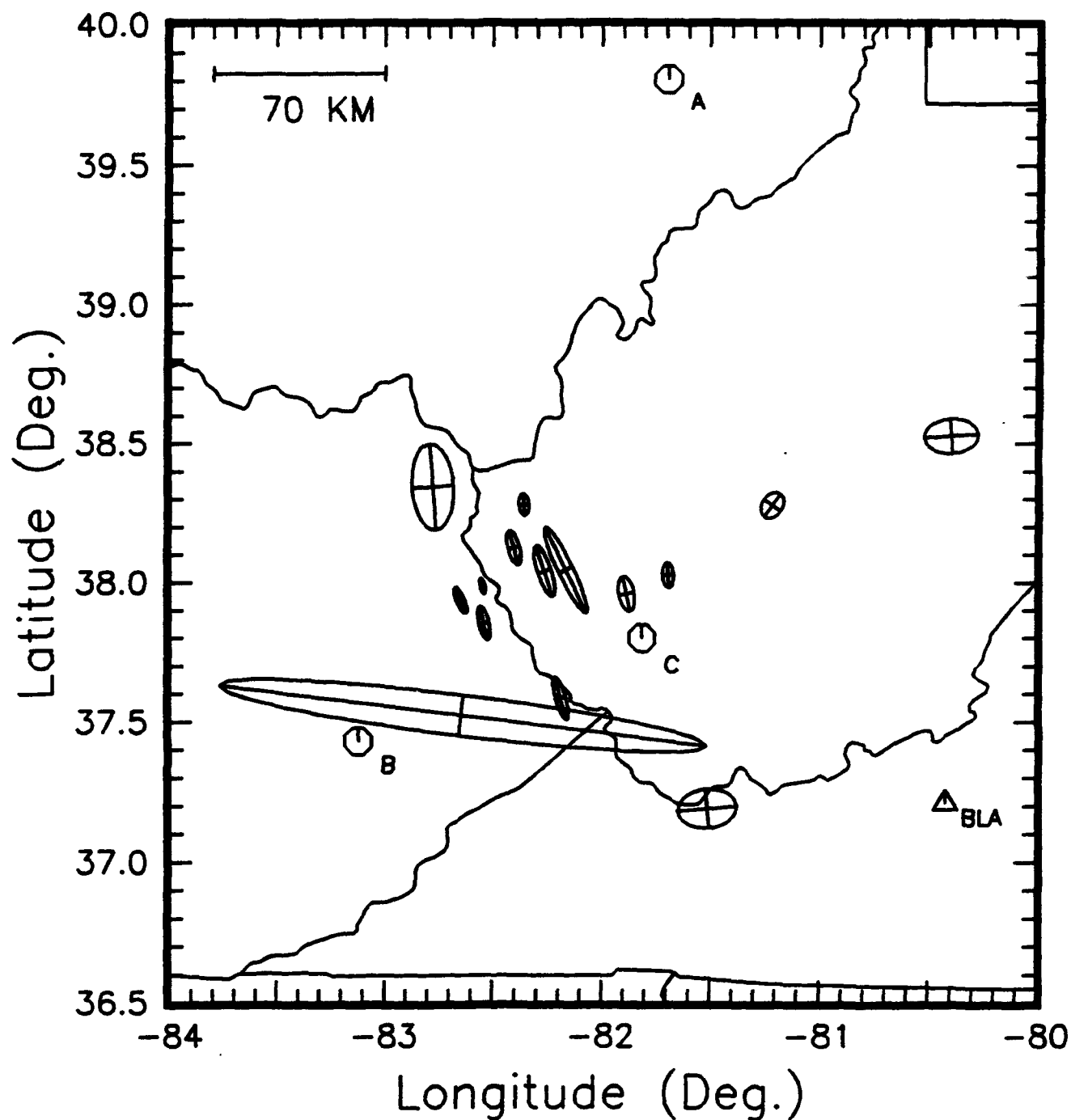


Figure 3. Confirmed mine locations are shown by the circles with associated letters as listed in Table 1. The location of the three-component station is shown by the triangle. The ellipses indicate the horizontal projections of the HYPOELLIPSE 68% chi-square confidence ellipsoids for mine locations inferred from blast epicenters.

5. Method of P-Wave Polarization Analysis

The P-wave backazimuth estimates from the three-component BLA station were derived using the method developed by Jurkevics (1988). The processing is carried out in the time domain using a series of overlapping time windows. For each time window, a 3 x 3 data covariance matrix is formed from the auto- and cross-variances of the three components of motion. The principle axes of the polarization ellipsoid, $(\lambda_i u_i, i = 1, 2, 3)$ for each window are determined by solving the eigenproblem for eigenvalues $(\lambda_1, \lambda_2$ and $\lambda_3)$ and eigenvectors $(u_1, u_2,$ and $u_3)$. For P-wave motion, the azimuth of propagation is estimated from the horizontal orientation of the eigenvector corresponding to the largest eigenvalue, u_1 :

$$\text{Pazimuth} = \tan^{-1} (u_2/u_3), \quad (1)$$

where u_{j1} , $j = 1, 2, 3$ are the direction cosines of the eigenvector associated with the largest eigenvalue. A measure of the degree of rectilinearity of the particle motion is given by

$$R = 1 - \left((\lambda_2 + \lambda_3) / 2\lambda_1 \right), \quad (2)$$

which is 1.0 when λ_2 and λ_3 are zero, for pure P-wave motion. The method can be made frequency dependent by applying the analysis to narrow bandpassed time series data.

6. P-Wave Data Analysis

The BLA short-period data were corrected for minor differences in system response of the three component channels. Frequency domain assessment of the P-wave to pre-P-wave signal/noise levels was made by calculating the Fourier amplitude spectrum of the P-wave and pre-P-wave data segments using 10 sec time windows. Explosions with signal/noise ratios less than 2 in the frequency range 1 to 10 Hz were rejected. The three component data were then bandpass filtered using a four-pole Butterworth filter with corner frequencies 1.0 and 10.0 Hz.

The duration of the moving time window used in the polarization analysis is a critical parameter for determining accurate backazimuth estimates from the P-wave arrivals. Its value will depend upon the bandwidth of the signal, the sample rate and the polarization characteristics of the signal. Trial and error testing showed that a window duration of 0.5 seconds generally provided the best backazimuth determination with our data set. Given the data bandwidth of 1 to 10 Hz and a sample rate of 40 samples/second, windows less than 0.5 seconds in duration gave unstable results due to the small number of sample points, whereas larger windows tended to reduce resolution because of the non-stationary polarization character of the coda immediately following the initial P-wave arrival.

The polarization analysis was performed in an automated manner, with the best-estimate of the backazimuth determined on the basis of maximum rectilinearity near the time of initial P-wave motion.

Examples of the various steps involved in the processing procedure are shown in Figures 4 through 6. Shown in Figure 4 are the data from Explosion #16 at the Starfire Mine, rotated into vertical, radial and transverse components. Figure 5 shows the Fourier amplitude spectra of the 10 second P-wave and pre-P-wave noise segments. Figure 6 shows a 5 second duration sequence of the data centered near the time of P-wave onset, with continuous running estimates of backazimuth, rectilinearity and signal/noise ratio. The signal/noise quantity was calculated as the ratio of the average three-component amplitude in the 5 second moving window to the average long-term three-component amplitude using a 10 second data segment prior to P-wave onset.

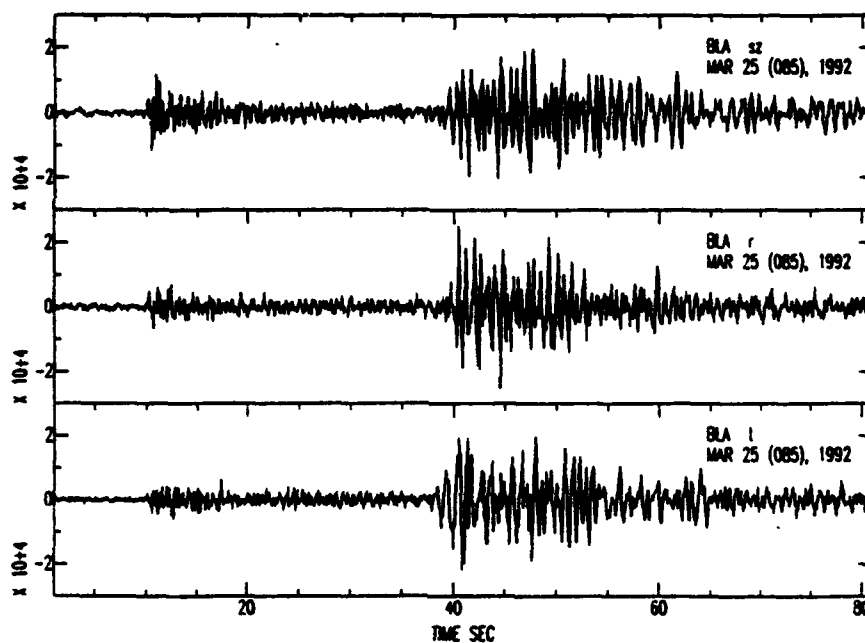


Figure 4. Time series data for Explosion #16 at the Starfire Mine in Kentucky. The data have been rotated into vertical (top), radial (center), and transverse (bottom) components.

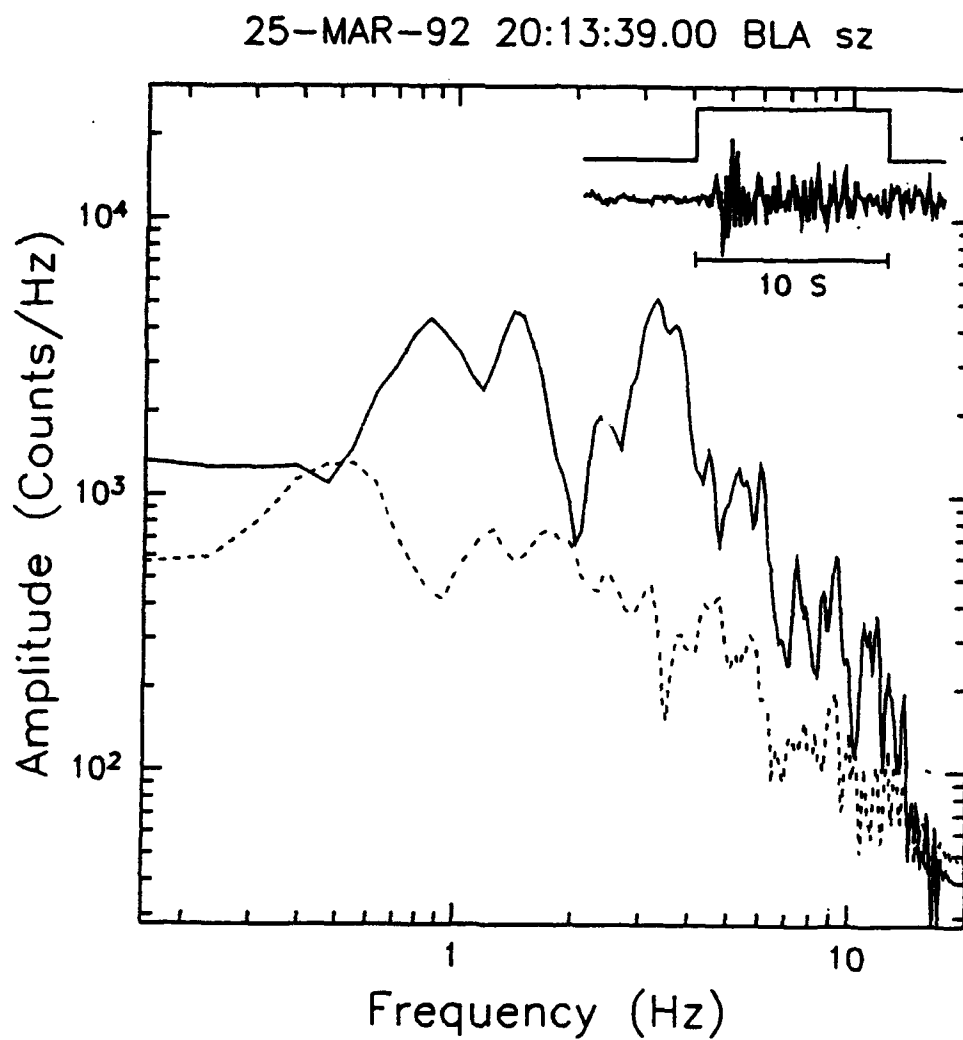


Figure 5. Fourier amplitude spectra of the vertical component P wave arrival, Explosion #16 (solid line), and the pre-P wave noise (dashed). Ten second time windows were used.

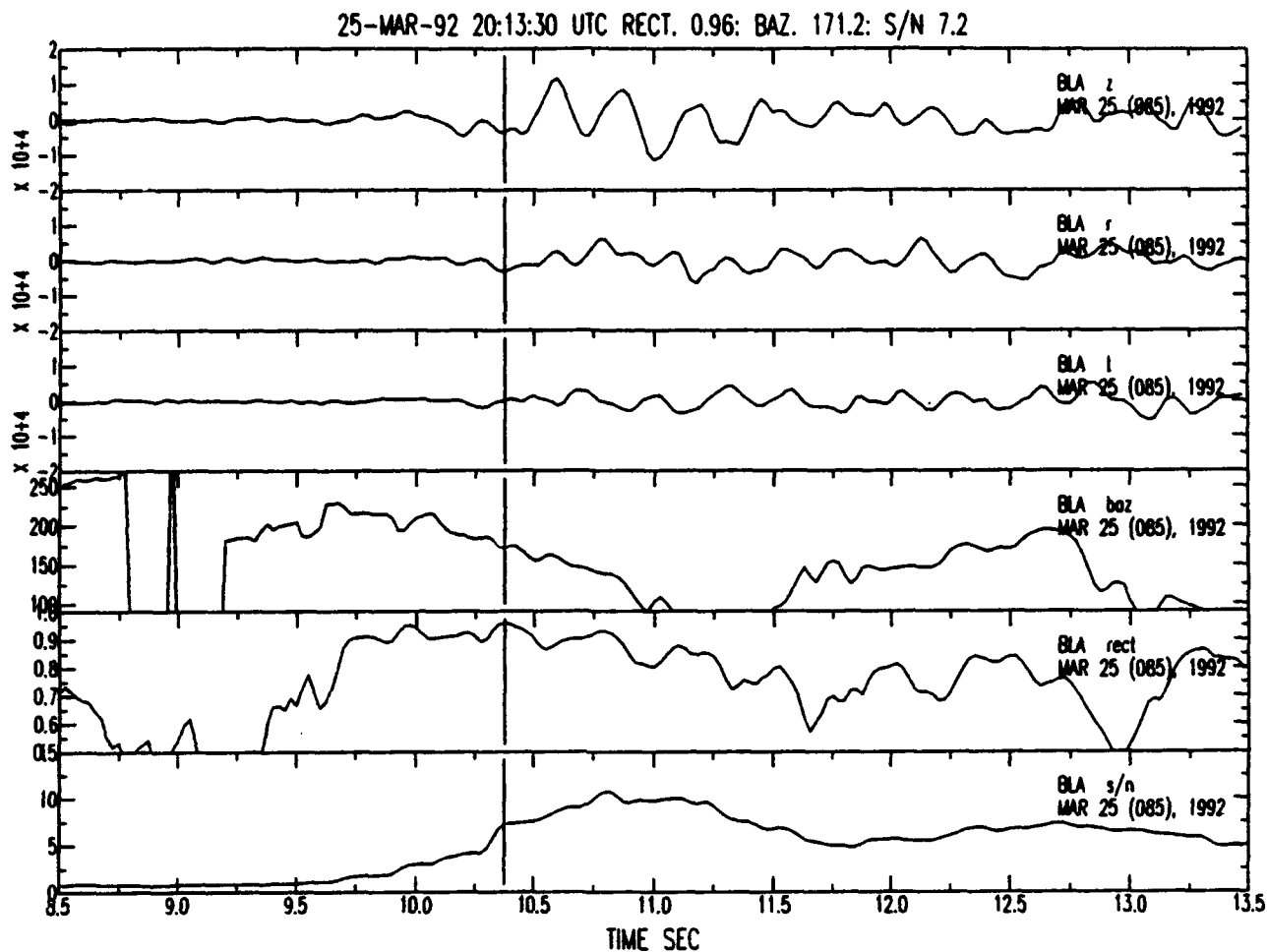


Figure 6. Results of polarization processing for Explosion #16. From the top, the traces are: (1) Vertical, (2) radial, (3) transverse, (4) station-source backazimuth (deg), (5) rectilinearity, and (6) three-component signal/noise ratio. Note that for rotated components, the true backazimuth angle is 180 degrees. Vertical lines indicate time at which the rectilinearity is maximum. The duration of the moving window for polarization analysis is 0.5 seconds.

7. Results of the P-Wave Analysis

The backazimuth errors, defined as the differences in the network derived estimates and the results from the three-component P-wave polarization measurements, are plotted as functions of signal/noise ratio and rectilinearity in Figures 7 and 8, respectively. Figure 7 suggests that ratios less than 2 can, but do not always, result in very unstable estimates of the polarization parameters, as evidenced by the two points with backazimuth errors in excess of 90 degrees. These two events are #35 and #24 (Table 1). Note that other examples of explosions at both of these mines, featuring similar signal/noise ratios, produced backazimuth estimates much closer to the true values. An example involves Events 35 and 20, both at the Central Ohio Mine. Figures 9 and 10 show the three-component recordings for the explosions. Figures 11 and 12 show the vertical component P-wave and pre-P-wave noise spectra of the two signals, and Figures 13 and 14 summarize the three-component processing results for both events. Note that the moving window backazimuth estimates near the times of P-wave onset are stable at values near the true value of 180 degrees for the rotated components, in the case of Event 20 (Figure 14), whereas those for Event 35 (Figure 13) change rapidly at times near the P-wave onset. Clearly, the random changes in the character of the noise may severely affect the backazimuth determination, when the signal/noise ratio is small.

Large signal/noise ratios do not guarantee accurate backazimuth estimates, at least for BLA and this mine explosion data set. Figure 7 shows no evidence for the backazimuth error to decrease with increasing signal/noise ratio, in the range 2 to 10. Deleting the two observations with errors in excess of 100 degrees results in a mean azimuth error of -6 degrees; the standard deviation is 21 degrees.

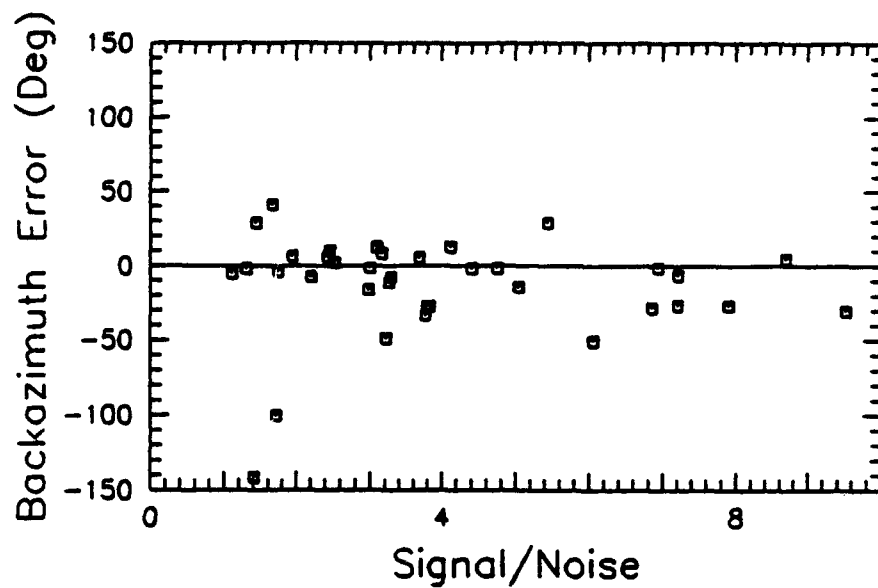


Figure 7. Three-component station backazimuth error versus signal/noise ratio.

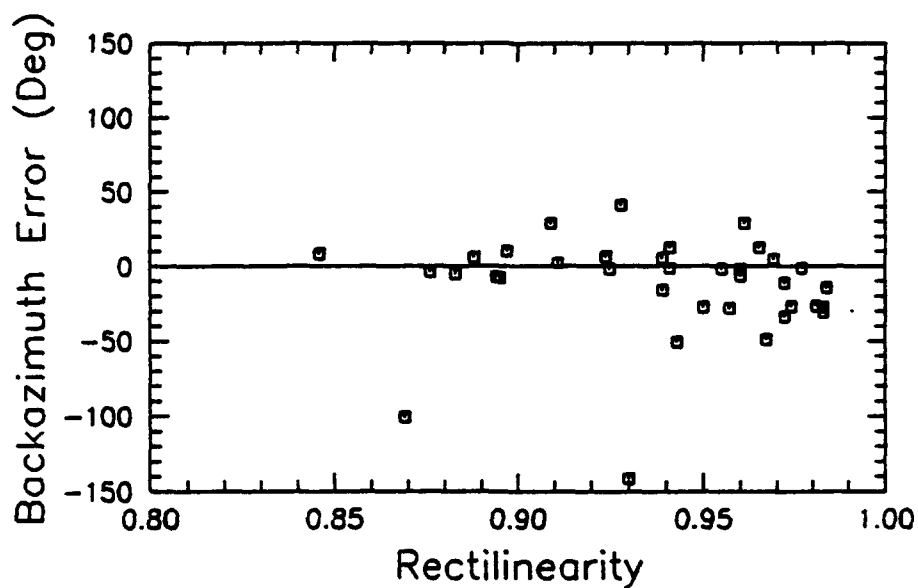


Figure 8. Three-component station backazimuth error versus rectilinearity.

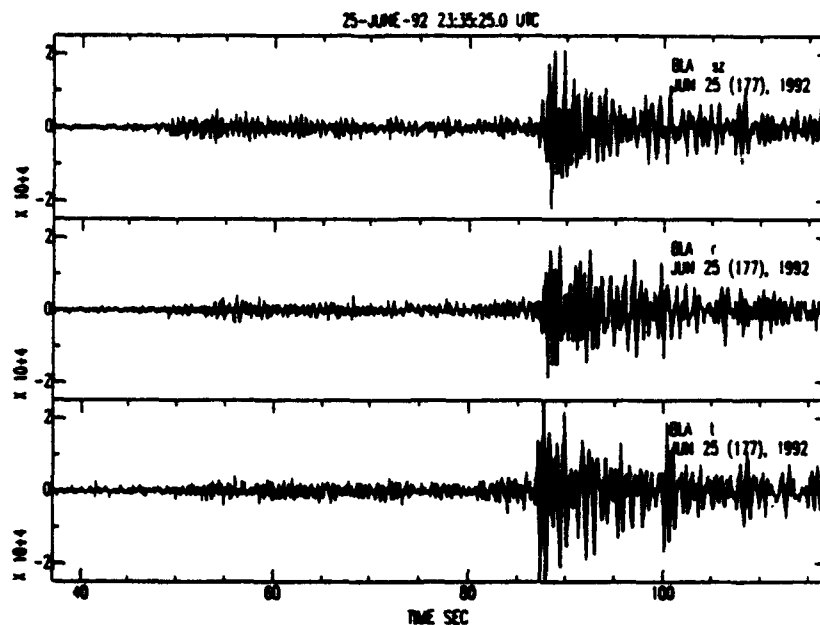


Figure 9. Time series data for Explosions #35 at the Central Ohio Mine. (Top) Vertical component, (middle) radial component, (bottom) transverse component.

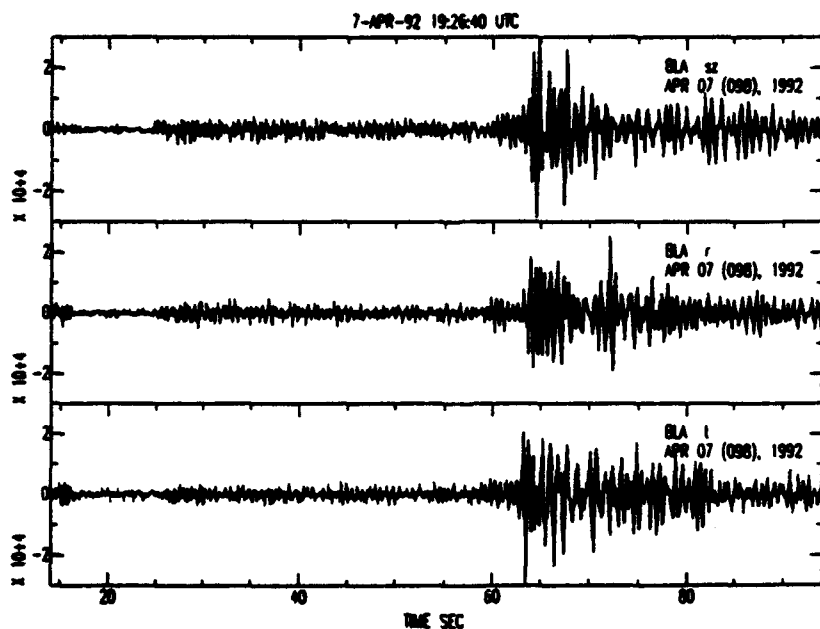


Figure 10. Time series data for Explosion #20 at the Central Ohio Mine. (Top) Vertical component, (middle) radial component, (bottom) transverse component.

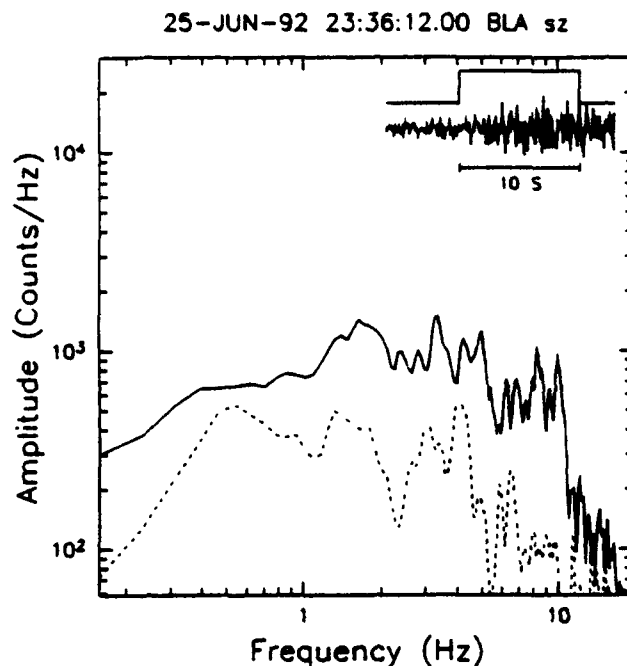


Figure 11. Fourier amplitude spectrum, Explosion #35: Vertical component P wave arrival (solid) and pre-P wave noise (dashed). Ten second time windows were used.

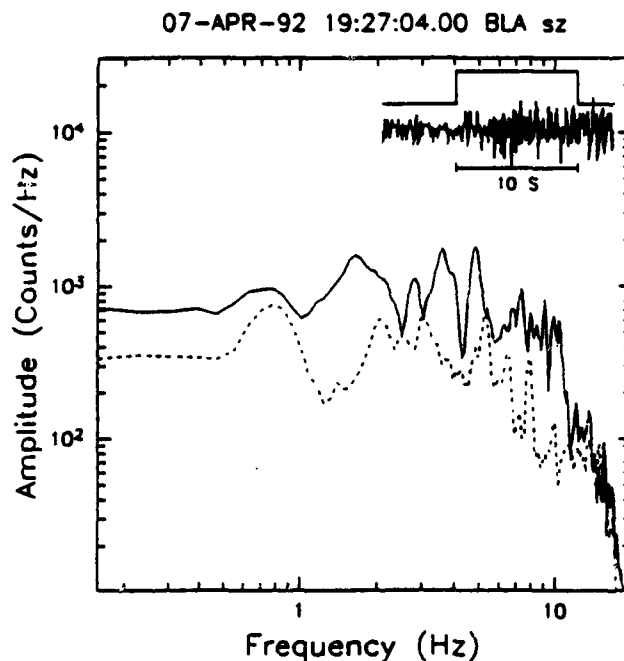


Figure 12. Fourier amplitude spectrum, Explosion #20: Vertical component P wave arrival (solid) and pre-P wave noise (dashed). Ten second time windows were used.

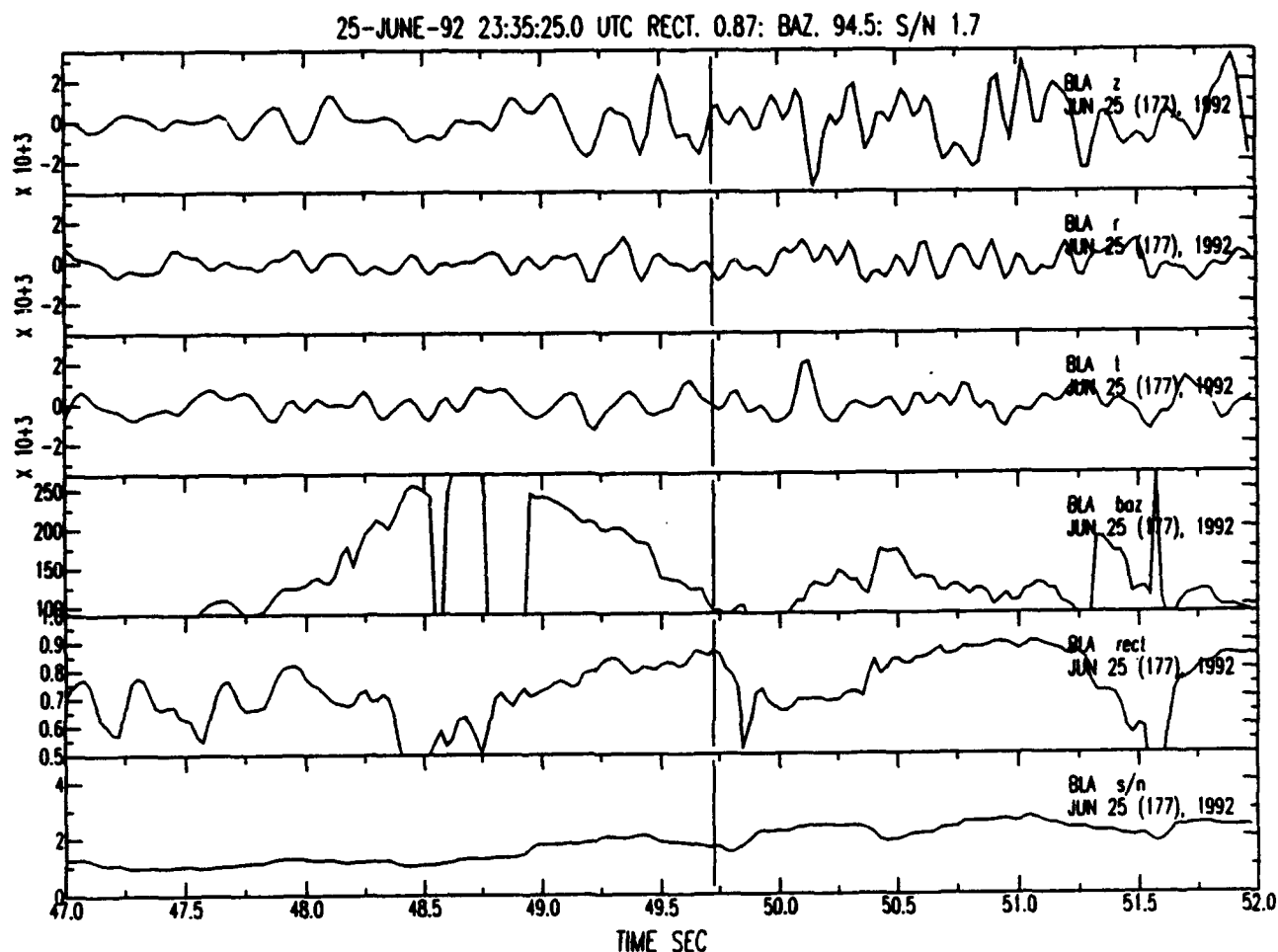


Figure 13. Results of polarization processing for Explosion #35. From the top, the traces are: (1) Vertical, (2) radial, (3) transverse, (4) station-source backazimuth (deg), (5) rectilinearity, and (6) three-component signal/noise ratio. Note that for rotated components, the true backazimuth angle is 180 degrees. Vertical lines indicate time at which the rectilinearity is maximum. The duration of the moving window for polarization analysis is 0.5 seconds.

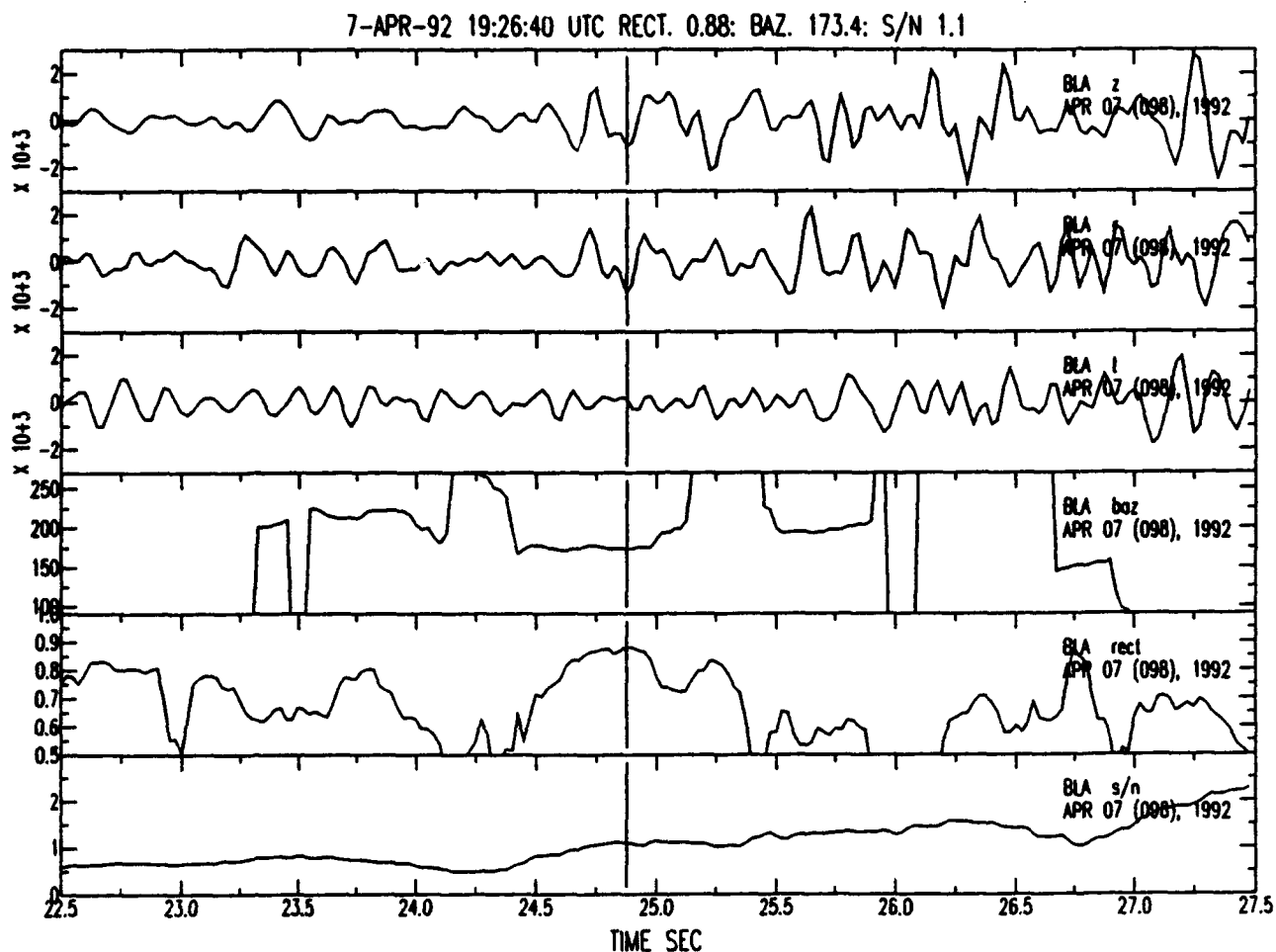


Figure 14. Results of polarization processing for Explosion #20. From the top, the traces are: (1) Vertical, (2) radial, (3) transverse, (4) station-source backazimuth (deg), (5) rectilinearity, and (6) three-component signal/noise ratio. Note that for rotated components, the true backazimuth angle is 180 degrees. Vertical lines indicate time at which the rectilinearity is maximum. The duration of the moving window for polarization analysis is 0.5 seconds.

Figure 8 shows the backazimuth error plotted as a function of rectilinearity. Again, there is no tendency in this data set for the errors to decrease with increasing values of this parameter in the range 0.8 to 1.0. Thus, it appears that the P-wave arrivals from some of the mine explosions are arriving from off-azimuth directions, possibly due to refraction from laterally heterogeneous velocity structure.

As a rule, the explosion data set exhibits very emergent and complex P-wave arrivals. The emergent character of the signal may be due to the extended nature of the delay-fired source-time function. For example, typical large explosions at the Starfire Mine involve up to 60 separate charges, and the duration of the source time function can be in excess of 1 second (Chapman, et al., 1992). This is also the case for some of the larger explosions at the Ruffner Mine (personal communication, mine engineers) and is probably typical of most of the explosions in our data set from other mines as well. Results from the polarization analysis indicate that, in general, only the initial portion of the P-wave arrival exhibits strongly rectilinear motion, which is polarized in the source-station azimuth. Off-azimuth arrivals consisting of converted and scattered energy appear at a very early stage in the coda: rarely can accurate estimates of the P-wave backazimuth be obtained from portions of the coda at times greater than 1.0 second following the initial onset time. Also, as shown in Figure 15, the P-wave angles of incidence with the vertical are small, averaging 22 degrees with a standard deviation of 9 degrees. This results in a reduced signal/noise ratio on the horizontal components, which is approximately one-half of the total three-component value given in Table 1. This phenomenon, which may be station dependent, tends to further reduce the accuracy of the backazimuth determination for low S/N events.

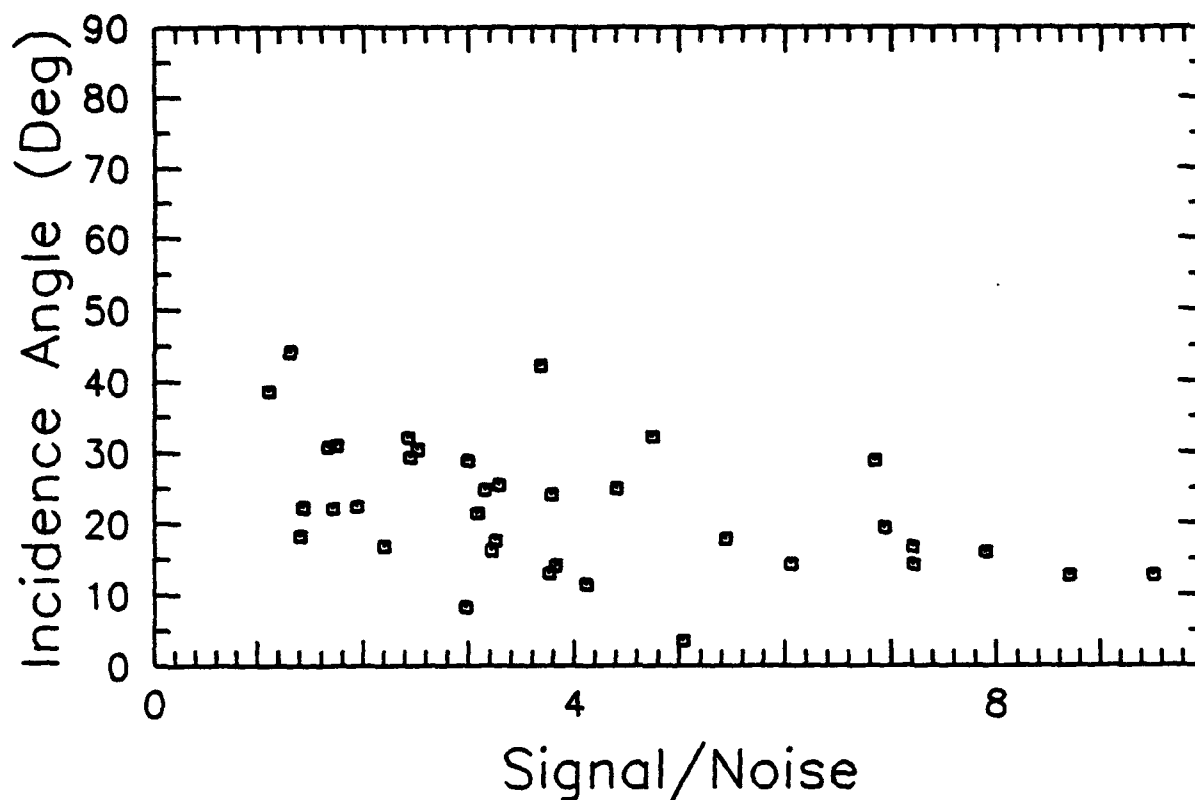


Figure 15. Apparent angle of incident P wave versus three-component signal/noise ratio.

Figures 16 through 27 show five examples with signal/noise ratios exceeding 4 wherein the polarization analysis resulted in backazimuth estimates correct to within 10 degrees of the true value. Note that in most cases, the very early portion of the signal yielded the best estimate of the backazimuth, and that the polarization characteristics of the immediate P-wave coda tend to fluctuate strongly.

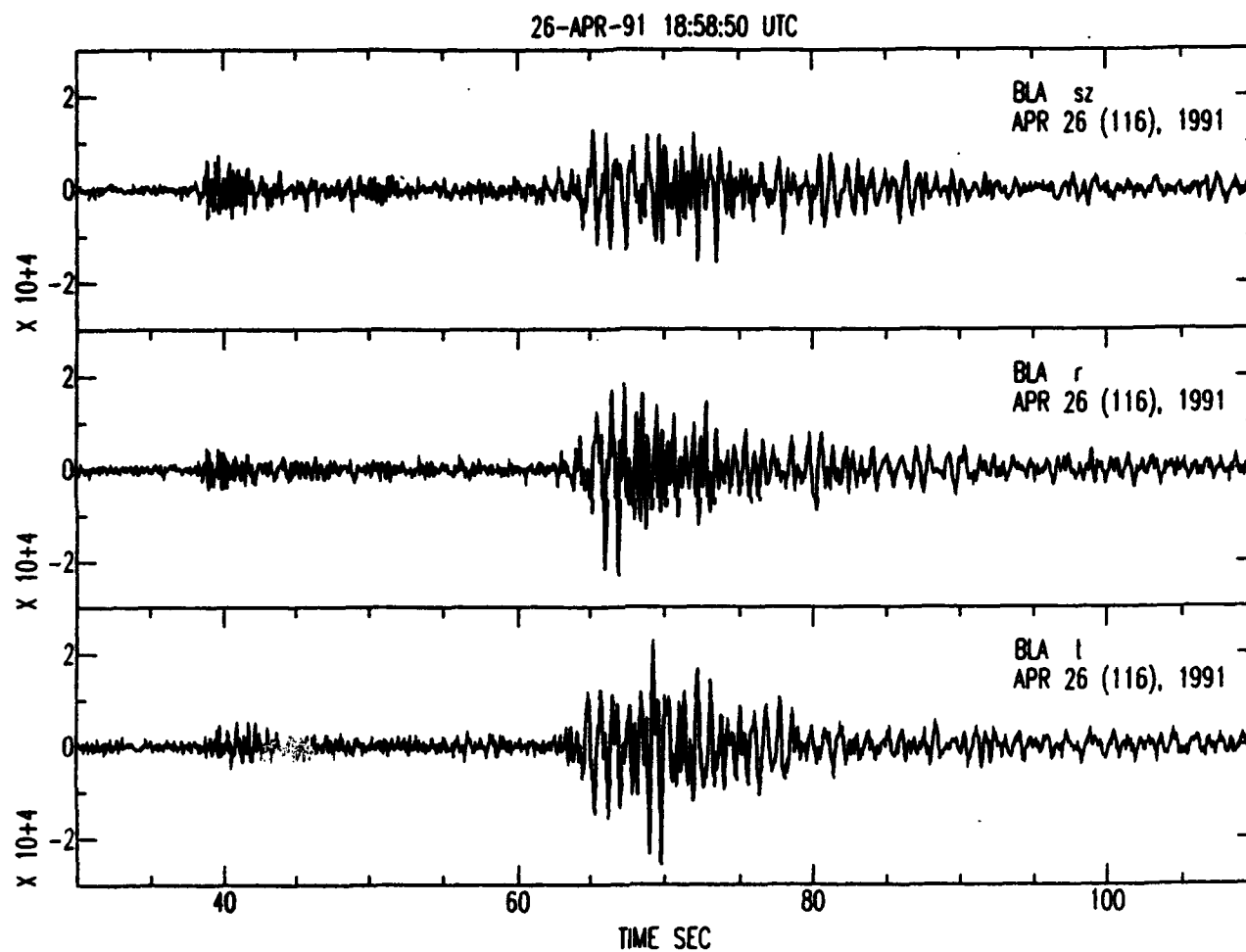


Figure 16. Time series data for Explosion #9. (Top) Vertical component, (middle) radial, (bottom) transverse.

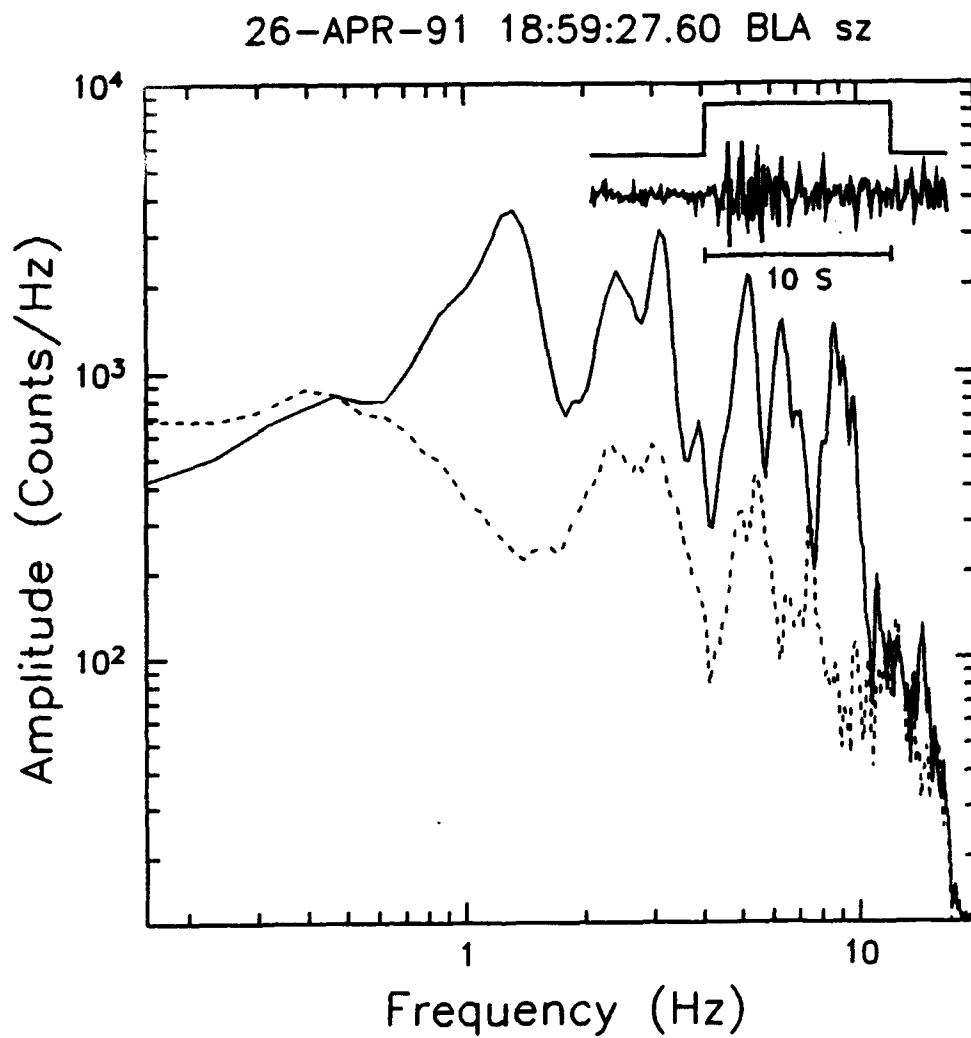


Figure 17. Fourier amplitude spectrum, Explosion #9: Vertical component P wave arrival (solid) and pre-P wave noise (dashed). Ten second time windows were used.

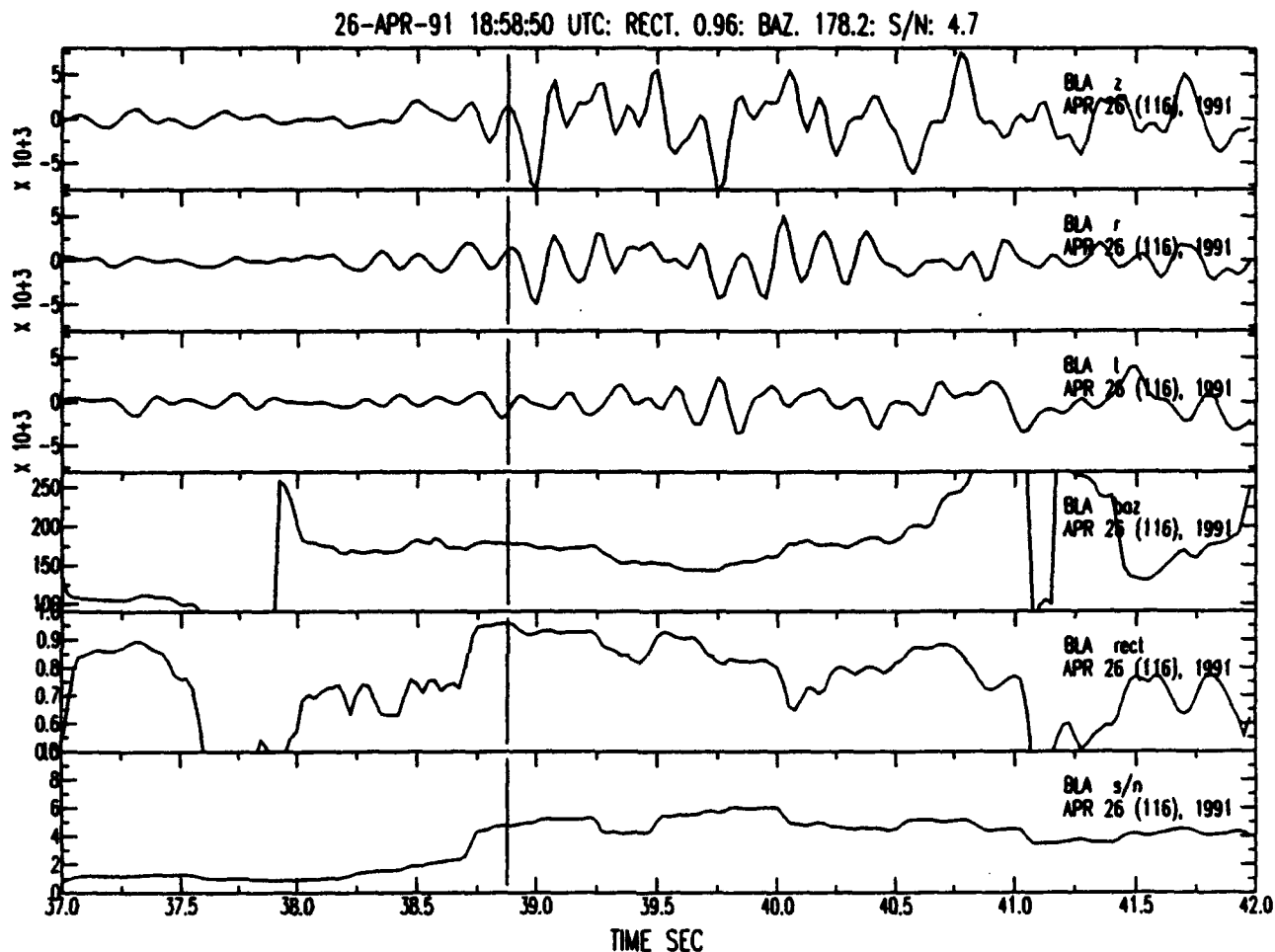


Figure 18. Results of polarization processing for Explosion #9. From the top, the traces are: (1) Vertical, (2) radial, (3) transverse, (4) station-source backazimuth (deg), (5) rectilinearity, and (6) three-component signal/noise ratio. Note that for rotated components, the true backazimuth angle is 180 degrees. Vertical lines indicate time at which the rectilinearity is maximum. The duration of the moving window for polarization analysis is 0.5 seconds.

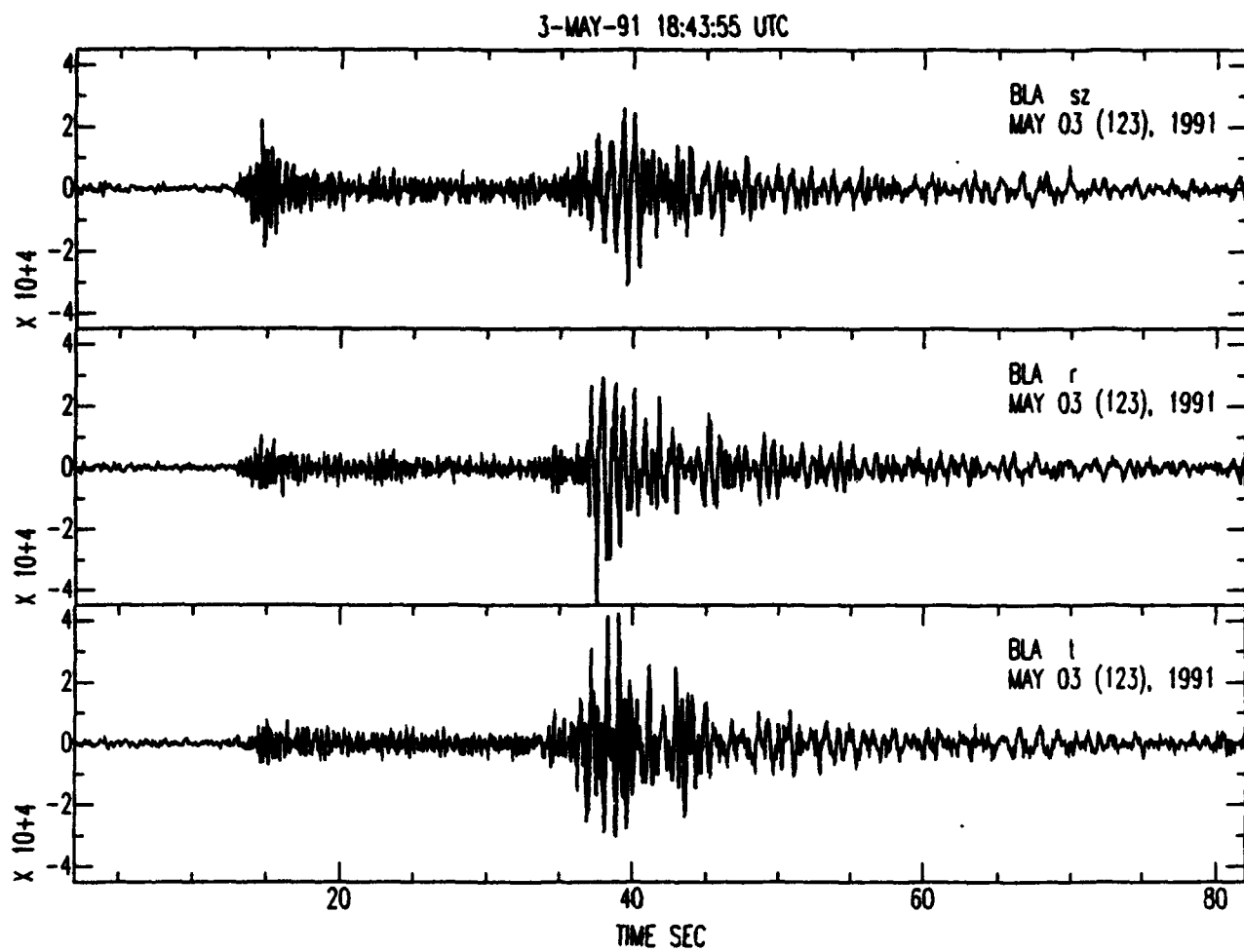


Figure 19. Time series data for Explosion #12. (Top) Vertical component, (middle) radial, (bottom) transverse.

03-MAY-91 18:44:07.00 BLA sz

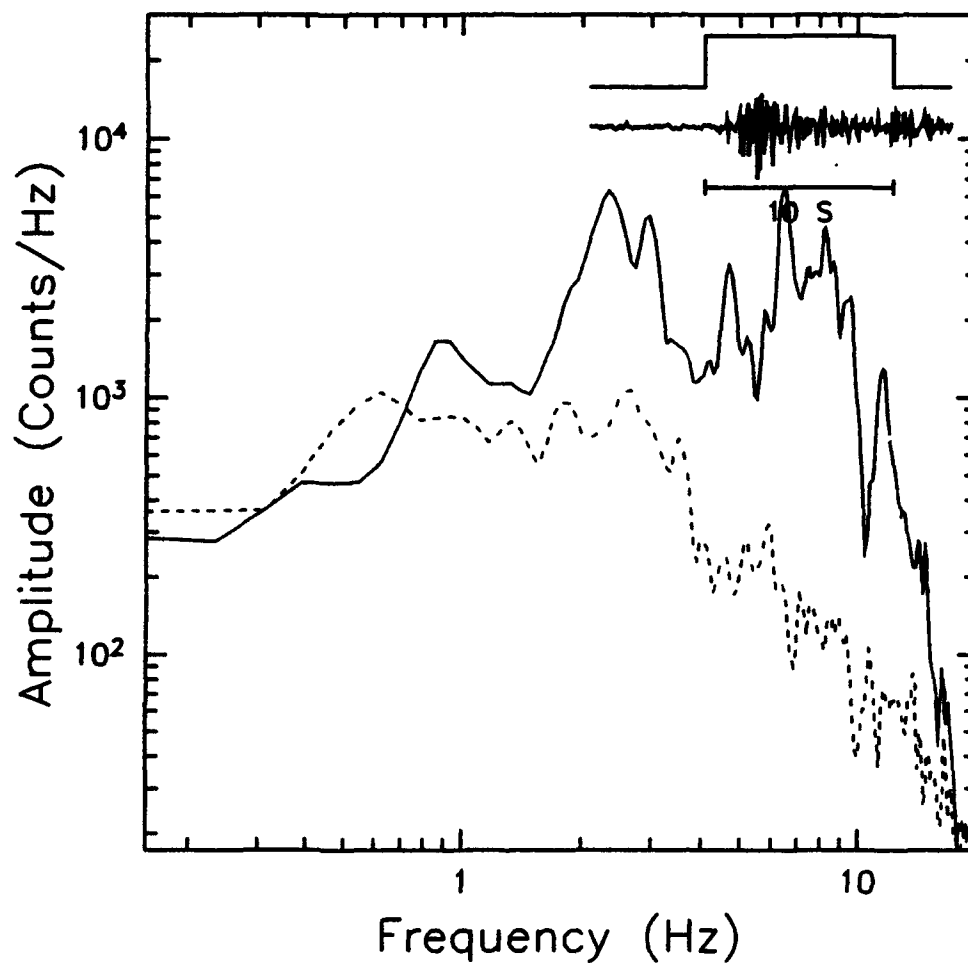


Figure 20. Fourier amplitude spectrum, Explosion #12: Vertical component P wave arrival (solid) and pre-P wave noise (dashed). Ten second time windows were used.

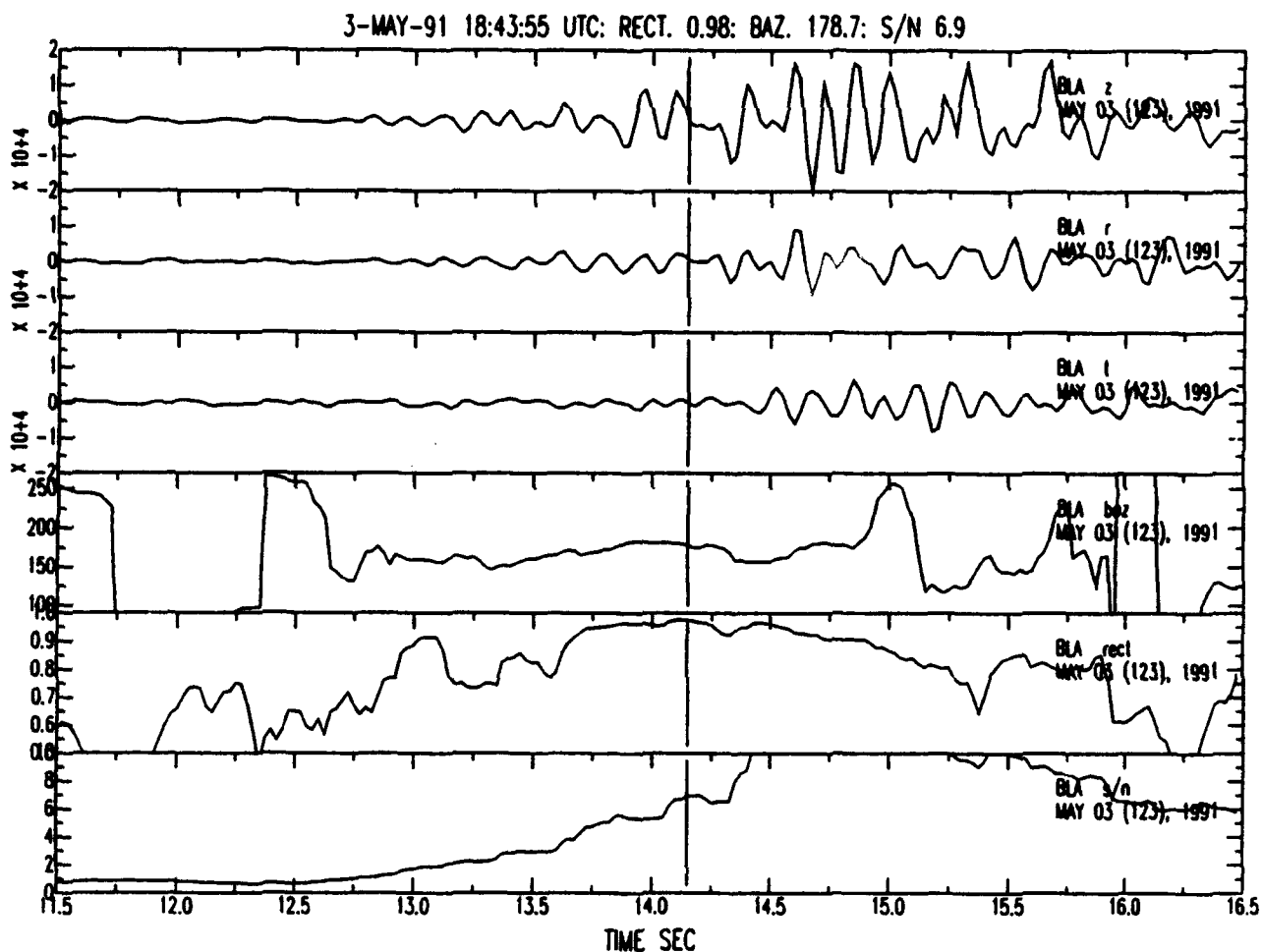


Figure 21. Results of polarization processing for Explosion #12. From the top, the traces are: (1) Vertical, (2) radial, (3) transverse, (4) station-source backazimuth (deg), (5) rectilinearity, and (6) three-component signal/noise ratio. Note that for rotated components, the true backazimuth angle is 180 degrees. Vertical lines indicate time at which the rectilinearity is maximum. The duration of the moving window for polarization analysis is 0.5 seconds.

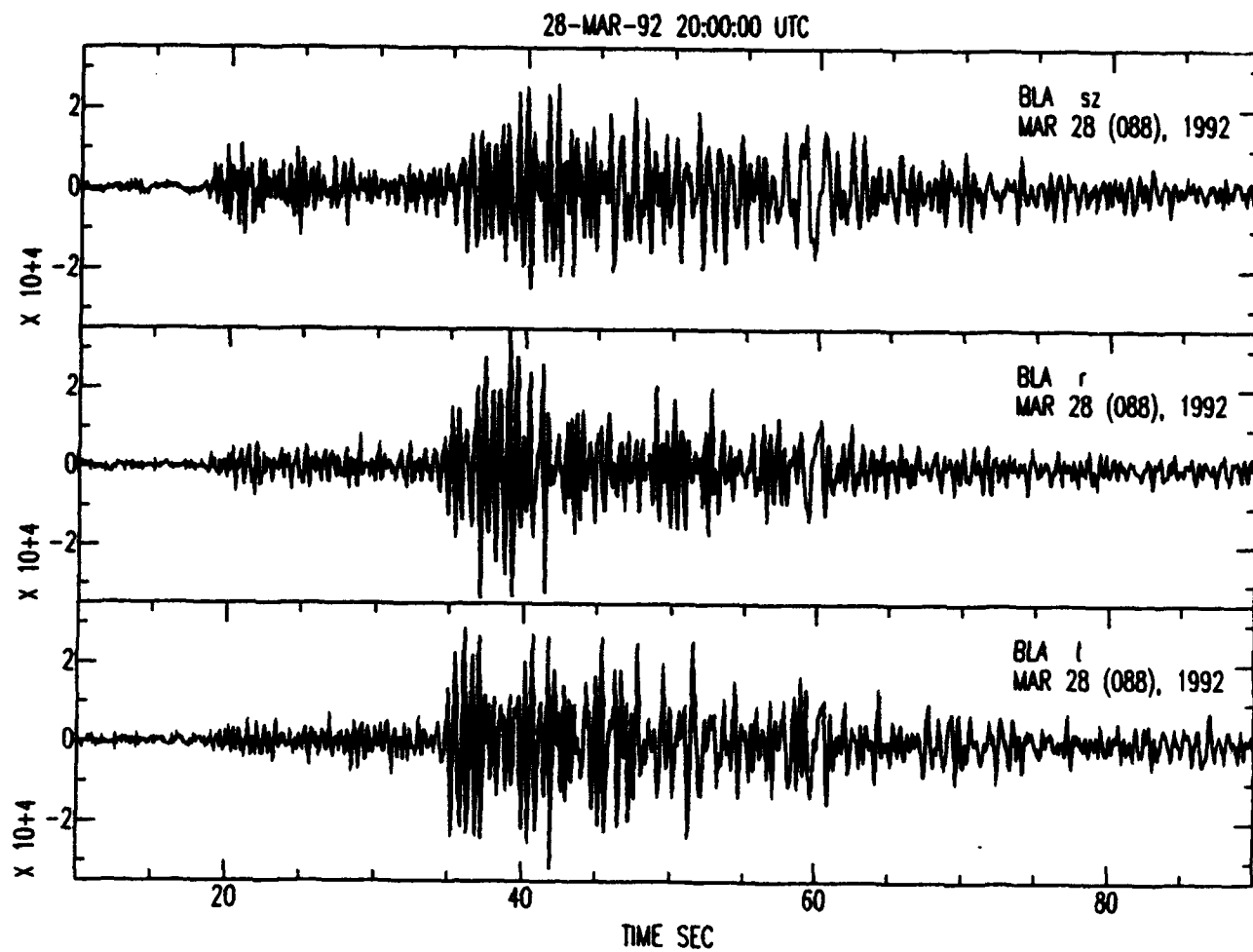


Figure 22. Time series data for Explosion #17. (Top) Vertical component, (middle) radial, (bottom) transverse.

28-MAR-92 20:00:17.00 BLA sz

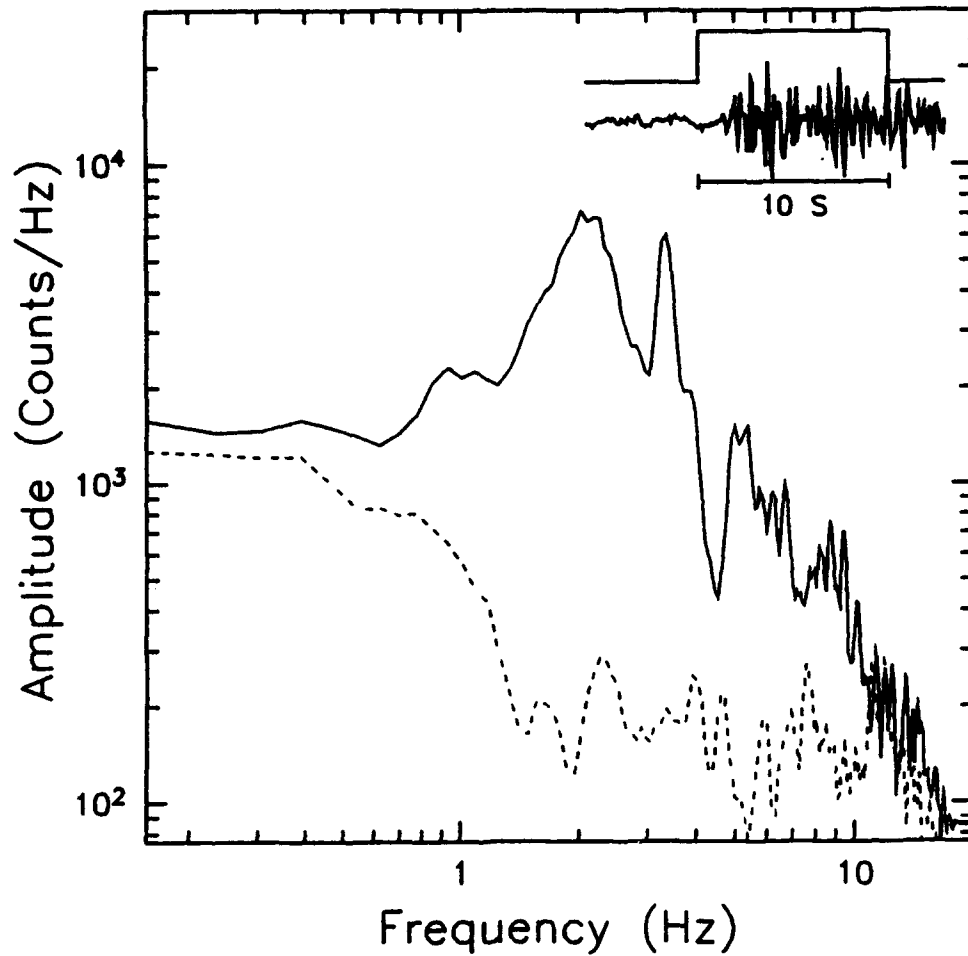


Figure 23. Fourier amplitude spectrum, Explosion #17: Vertical component P wave arrival (solid) and pre-P wave noise (dashed). Ten second time windows were used.

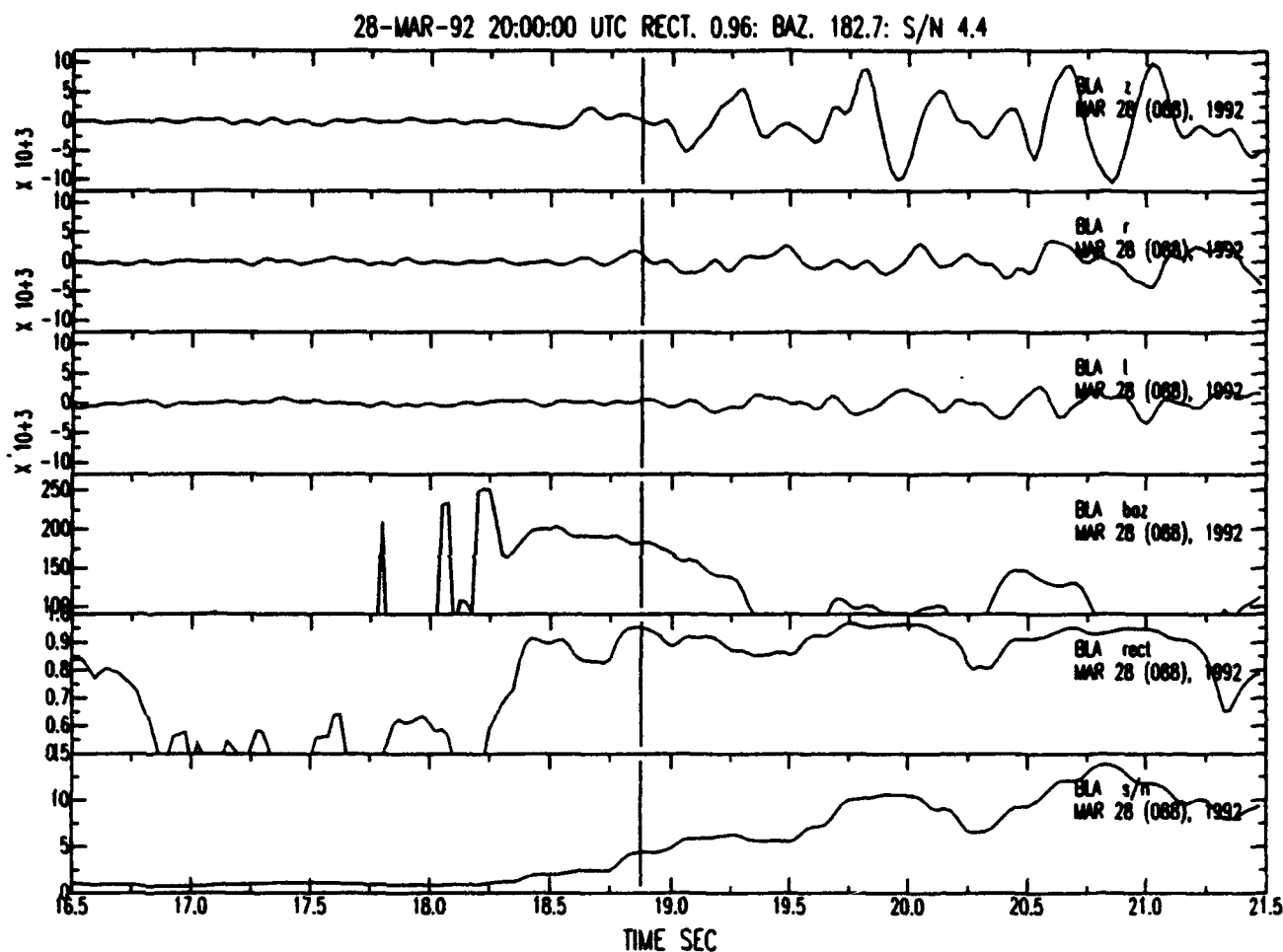


Figure 24. Results of polarization processing for Explosion #17. From the top, the traces are: (1) Vertical, (2) radial, (3) transverse, (4) station-source backazimuth (deg), (5) rectilinearity, and (6) three-component signal/noise ratio. Note that for rotated components, the true backazimuth angle is 180 degrees. Vertical lines indicate time at which the rectilinearity is maximum. The duration of the moving window for polarization analysis is 0.5 seconds.

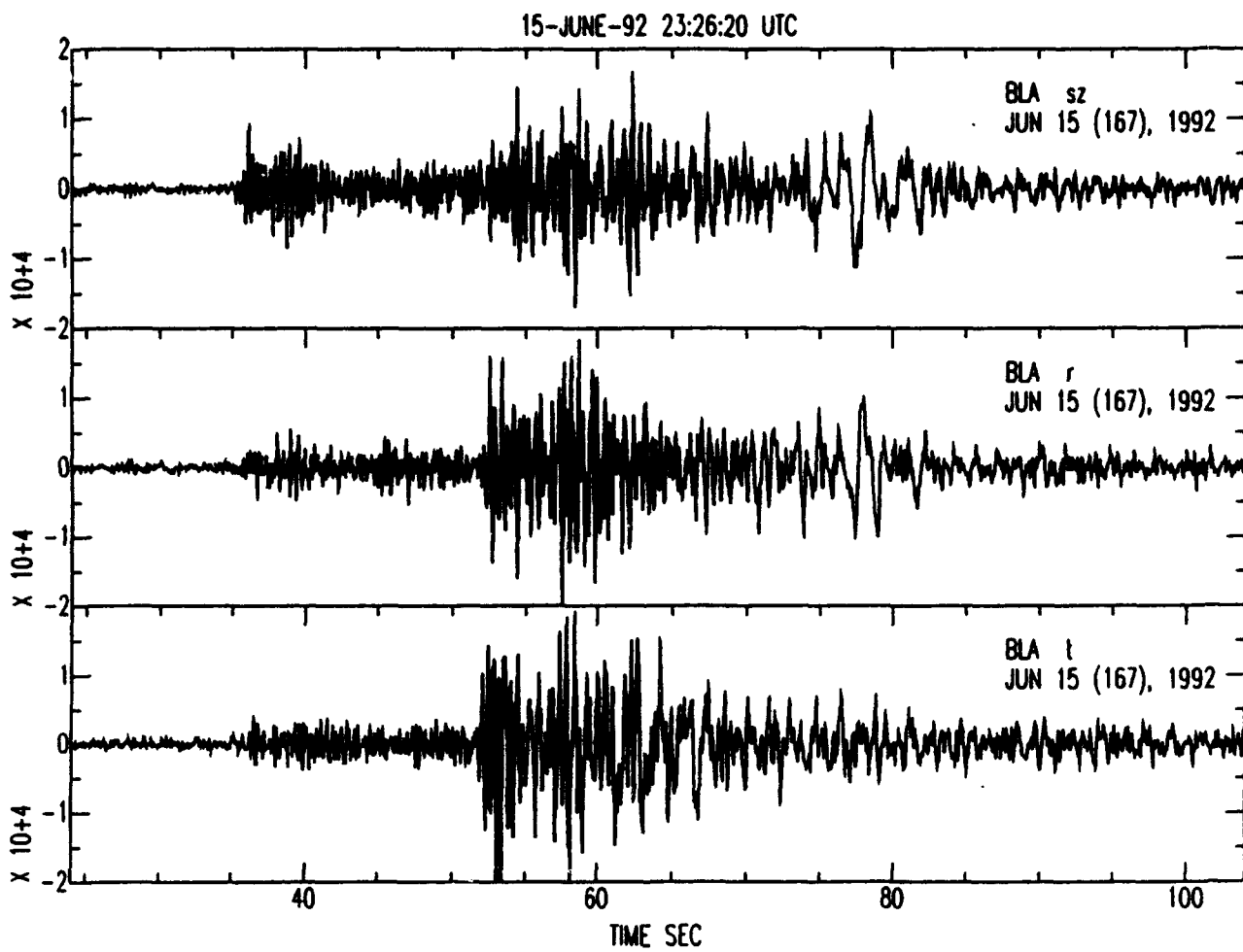


Figure 25. Time series data for Explosion #33. (Top) Vertical component, (middle) radial, (bottom) transverse.

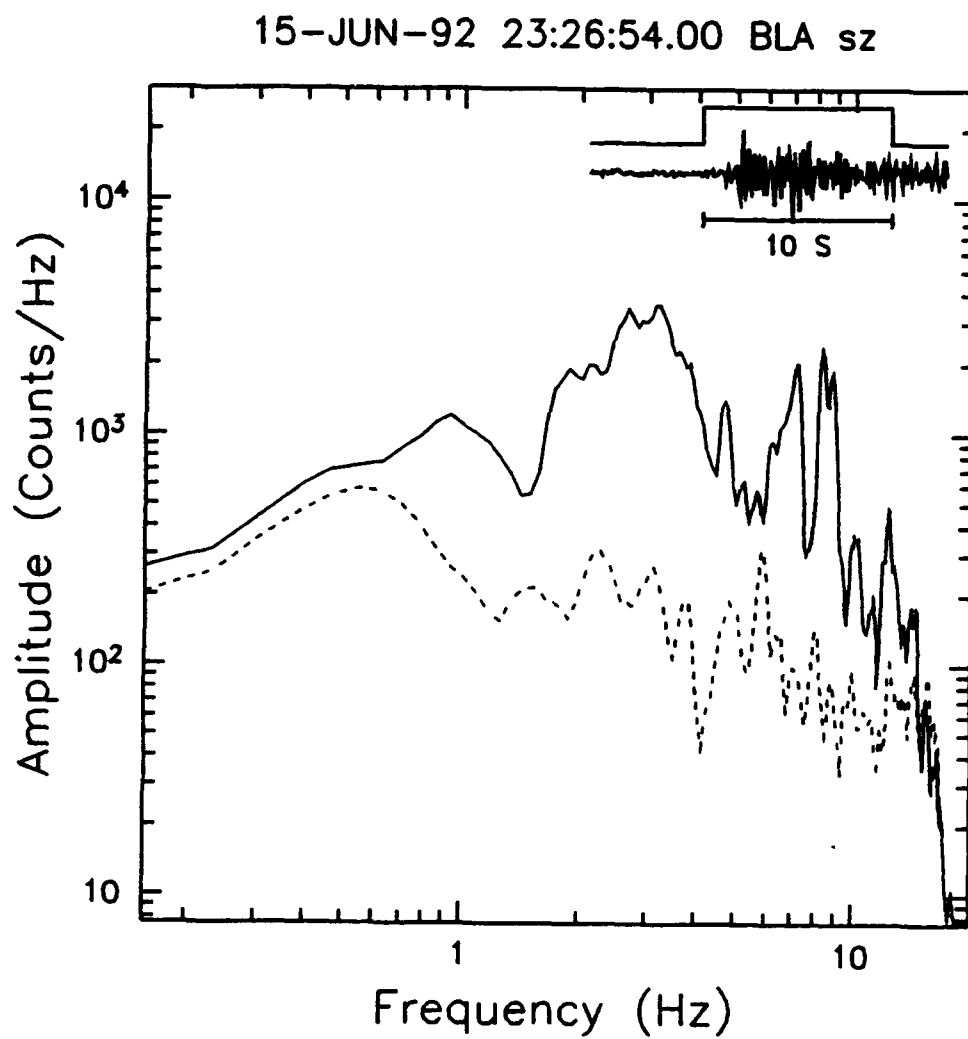


Figure 26. Fourier amplitude spectrum, Explosion #33: Vertical component P wave arrival (solid) and pre-P wave noise (dashed). Ten second time windows were used.

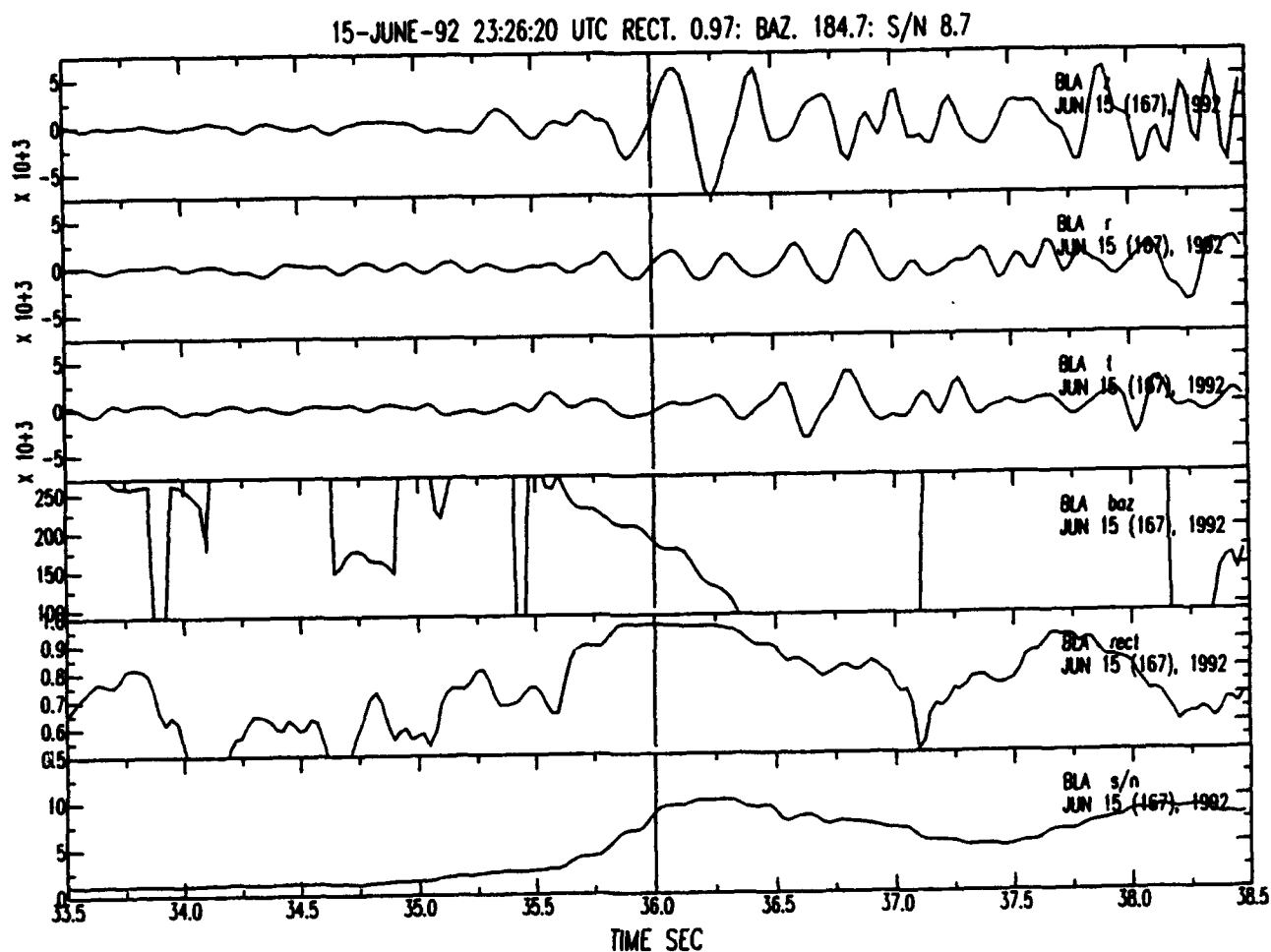


Figure 27. Results of polarization processing for Explosion #33. From the top, the traces are: (1) Vertical, (2) radial, (3) transverse, (4) station-source backazimuth (deg), (5) rectilinearity, and (6) three-component signal/noise ratio. Note that for rotated components, the true backazimuth angle is 180 degrees. Vertical lines indicate time at which the rectilinearity is maximum. The duration of the moving window for polarization analysis is 0.5 seconds.

8. Rg-Wave Analysis

The complications discussed above make accurate backazimuth determination difficult for this delay-fired explosion data set. In an effort to extract more information from the single-station data, we have examined the potential for using the Rg phase to determine source direction.

Several of the explosion signals exhibit Rg phases. At BLA, Rg is a Rayleigh wave with group velocities in the range 1.8 to 2.3 km/sec. It is apparent on short period recordings which have been bandpass filtered for the range 0.2 to 1.0 Hz.

The backazimuth of the source was estimated from the Rg-wave by noting that for a laterally homogeneous, isotropic earth, the phase angles of the Rg radial component Fourier harmonics lead those of the vertical by 90 degrees. In the presence of noise and other seismic phases, this phase difference can be used to estimate the backazimuth if energy on the transverse component in the Rg frequency band is sufficiently incoherent with respect to that on the vertical and radial components. The approach we have used is described below.

9. Method of Rg-Wave Polarization Analysis

Let $z(\omega)$, $n(\omega)$ and $e(\omega)$ be the Fourier transforms of the windowed time series containing the Rg arrival on the vertical, north-south and east-west components. For an arbitrary rotation angle ϕ , representing a trial source-station azimuth, the radial component of motion is given by

$$r(\omega) = n(\omega) \cos(\phi) + e(\omega) \sin(\phi), \quad (3)$$

and the phase spectrum is

$$\Theta_r(\omega) = \arg r(\omega). \quad (4)$$

Similarly, for the vertical component, the phase is

$$\Theta_z(\omega) = \arg z(\omega). \quad (5)$$

Because the Rg signal is bandlimited, we define ω_j to represent the j 'th discrete Fourier frequency in the range $\omega_n \leq \omega_j \leq \omega_m$, $j = n, n+1, \dots, m$, where ω_n and ω_m are the lower and upper bandlimits of the signal.

Let

$$A_j = \sqrt{|z(\omega_j)|^2 + |r(\omega_j)|^2}, \text{ if } \left| [\Theta_r(\omega_j) - \Theta_z(\omega_j)] - \pi/2 \right| \leq \alpha$$

$$A_j = 0, \text{ if } \left| [\Theta_r(\omega_j) - \Theta_z(\omega_j)] - \pi/2 \right| > \alpha \quad (6)$$

where α is a pre-selected phase difference tolerance. By summing over the frequency band of interest, we obtain a measure of the coherent signal amplitude in the vertical-radial plane. This sum is normalized by the total three-component amplitude in the frequency band to yield

$$P = \sum_{j=n}^m A_j / \sqrt{|z(\omega_j)|^2 + |n(\omega_j)|^2 + |e(\omega_j)|^2}. \quad (7)$$

This quantity is unity when the rotation angle ϕ is such that all horizontal motion is in the radial direction, and the phase differences between radial and vertical Fourier harmonics in the chosen frequency band are in the range $\pi/2 \pm \alpha$. In practice, P is evaluated with ϕ ranging from 0 to 359 degrees, in 1 degree increments, with a phase difference tolerance of 10 degrees. The value of ϕ resulting in a maximum value of P is the estimated Rg azimuth of approach.

10. Results of the Rg-Wave Analysis

Twenty-seven signals exhibiting Rg arrivals were processed using the method described above. The calculated P values ranged from 0.08 to 0.76. Figures 28 through 31 show the results of analysis for four events. Figures 28 and 29 show results for explosions #22 and #19, respectively. These events feature the largest amplitude Rg arrivals in the data set. Figures 30 and 31 show results for explosions #11 and #29 which feature much smaller Rg arrivals. Note that the method is not highly dependent upon the amplitude of the Rg arrival. This is further illustrated in Figure 32 which plots the backazimuth error as a function of the parameter P. In some cases, good estimates of the backazimuth were found for P values as low as 0.08.

The backazimuths estimated from the Rg phase are compared with those derived from the P-wave in Figure 33. For Rg, the mean error is -2 degrees; the standard deviation is 26 degrees, which is only 5 degrees larger than the result obtained from the P-wave arrivals.

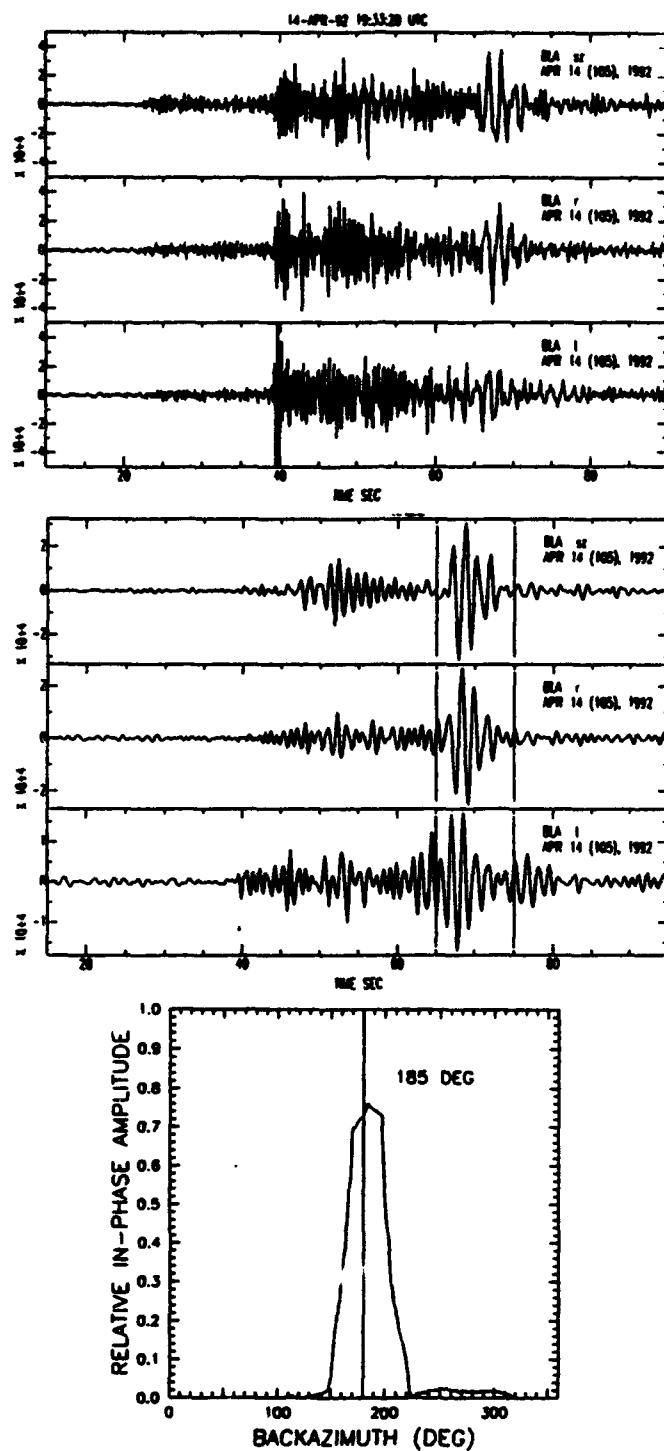


Figure 28. Results of Rg phase analysis for Explosion #22. (Top) Unfiltered series (vertical, radial, and transverse components). (Middle) Bandpass (0.2 to 1.0 Hz) filtered time series. The vertical lines indicate time segments used for analysis. (Bottom) Relative in-phase amplitude (parameter P in Equation 7) versus backazimuth (rotation angle ϕ). The vertical line indicates the true backazimuth of 180 degrees.

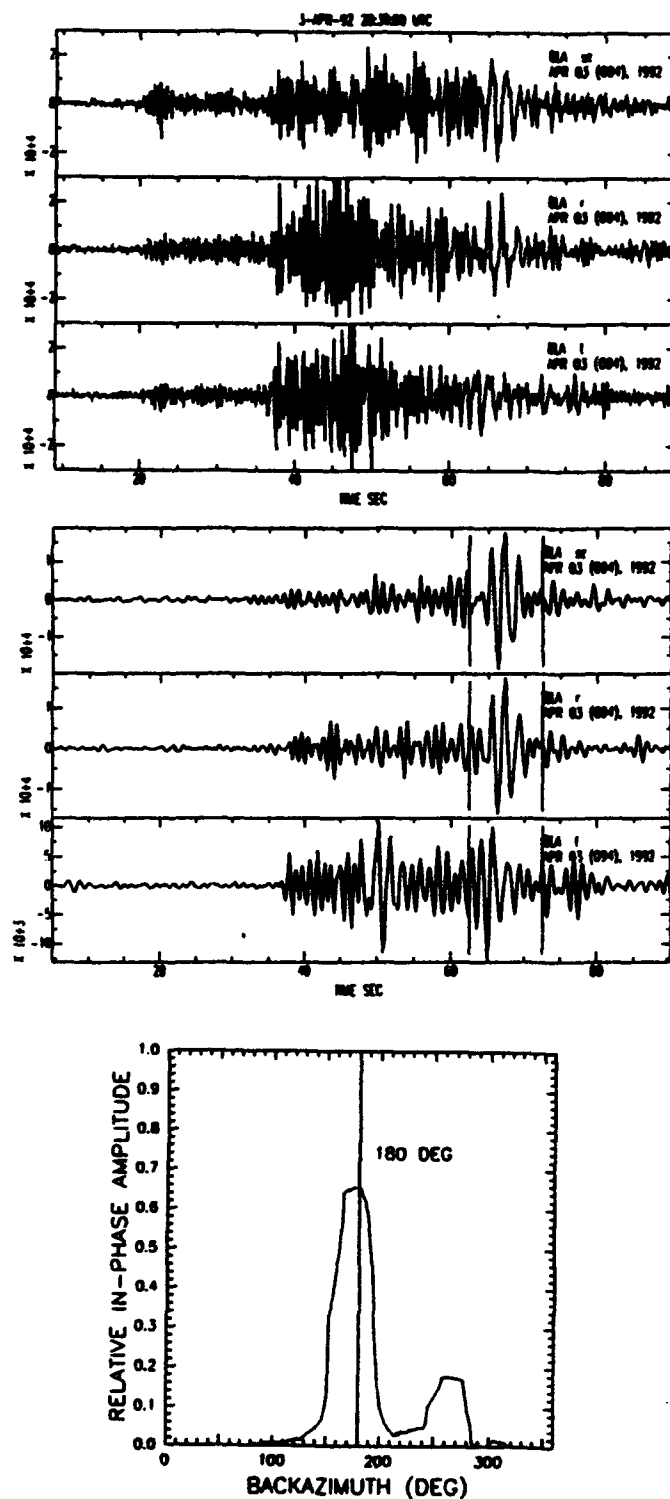


Figure 29. Results of Rg phase analysis for Explosion #19. (Top) Unfiltered series (vertical, radial, and transverse components). (Middle) Bandpass (0.2 to 1.0 Hz) filtered time series. The vertical lines indicate time segments used for analysis. (Bottom) Relative in-phase amplitude (parameter P in Equation 7) versus backazimuth (rotation angle ϕ). The vertical line indicates the true backazimuth of 180 degrees.

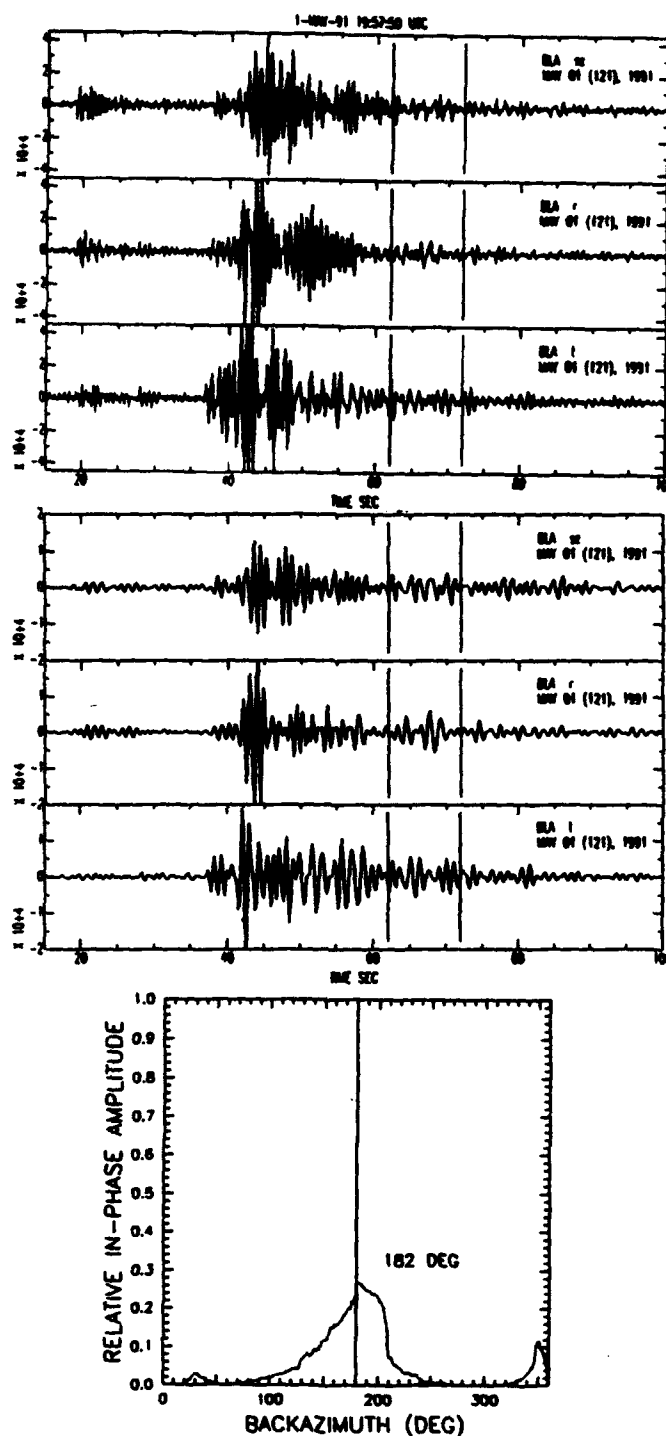


Figure 30. Results of Rg phase analysis for Explosion #11. (Top) Unfiltered series (vertical, radial, and transverse components). (Middle) Bandpass (0.2 to 1.0 Hz) filtered time series. The vertical lines indicate time segments used for analysis. (Bottom) Relative in-phase amplitude (parameter P in Equation 7) versus backazimuth (rotation angle ϕ). The vertical line indicates the true backazimuth of 180 degrees.

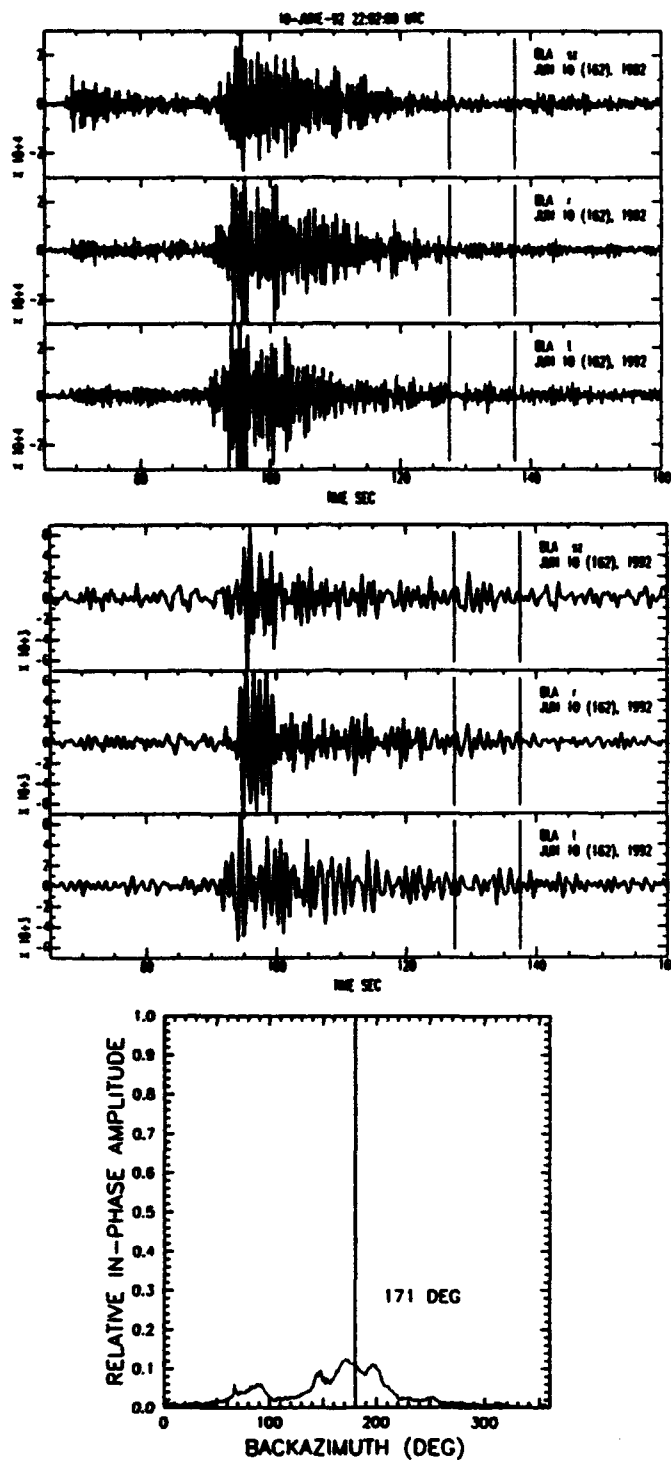


Figure 31. Results of Rg phase analysis for Explosion #29. (Top) Unfiltered series (vertical, radial, and transverse components). (Middle) Bandpass (0.2 to 1.0 Hz) filtered time series. The vertical lines indicate time segments used for analysis. (Bottom) Relative in-phase amplitude (parameter P in Equation 7) versus backazimuth (rotation angle ϕ). The vertical line indicates the true backazimuth of 180 degrees.

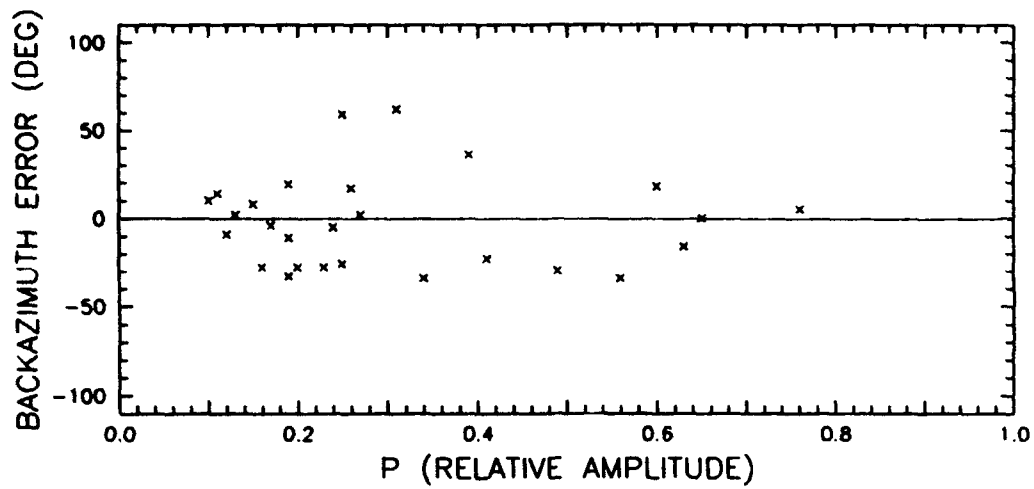


Figure 32. Rg phase backazimuth error versus relative amplitude parameter P .

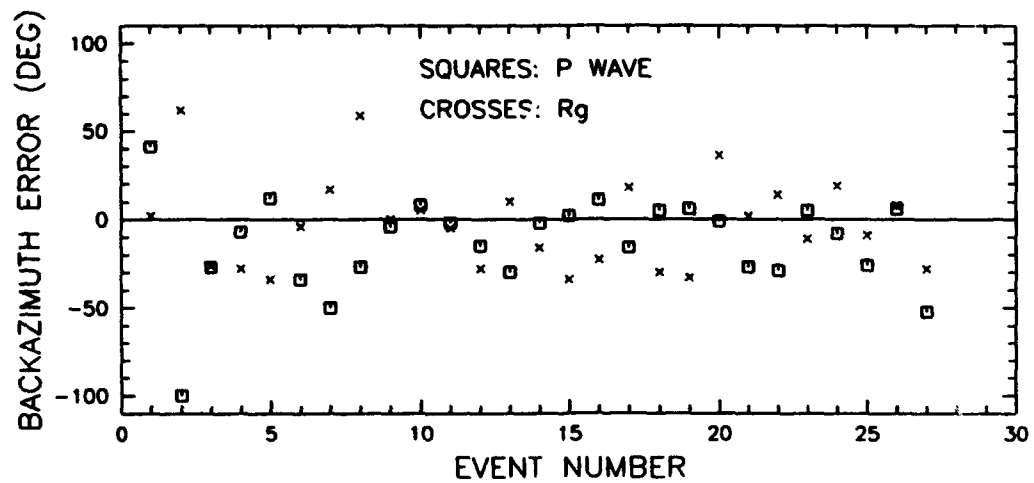


Figure 33. Backazimuth errors derived from P and Rg phases.

11. Conclusions and Recommendations

We have compared the single-station backazimuth estimates at BLA with independently derived locations for a set of mining explosions and find that for sources in the northwest quadrant, polarization analysis of the P-wave arrival gives an essentially unbiased estimate of the source direction (mean error 6 degrees), but that the scatter in the results is substantial with a standard deviation for 35 measurements of 21 degrees.

Characteristics of the P-wave signal which contribute to the errors in the estimates include: (1) emergent initial motions from the delay-fired explosions; (2) off-azimuth arrivals and/or converted phases arriving early in the P coda; (3) steep angles of incidence, averaging 22 degrees from vertical, which tend to reduce the signal/noise ratios on the horizontal components. Optimum data segments for reliable backazimuth estimates are restricted to short time intervals (1 second or less) beginning with the initial P-wave motion.

The Rg phase is present in many of the explosion signals at BLA. Analysis of this arrival using a phase difference criterion results in backazimuth estimates which, on average, have approximately the same reliability as those derived from the initial P-wave motion. It appears that this approach can often provide an alternative means of estimating the source direction, which could be important in situations where the P-wave signal/noise ratio is small.

12. References

- Bollinger, G. A., M. C. Chapman and T. P. Moore, (1980), Central Virginia regional seismic network: Crustal velocity structure in central and southwestern Virginia, NUREG/CR-1217, (R6, RA), U.S. NRC, Div. of Reactor Safety Res., Contract No. NRC-04-77-134, 187 pp.
- Chapman, M. C., G. A. Bollinger and M. S. Sibol, (1992), Modeling delay-fired explosion spectra at regional distances, Bull. Seism. Soc. Am., 82, pp. 2430-2447.
- Chapman, M. C., J. A. Snoke and G. A. Bollinger, (1988), A procedure for calibrating short-period telemetered seismograph systems, Bull. Seism. Soc. Am., 78, pp. 2077-2088.
- Jurkevics, A., (1988), Polarization analysis of three-component array data, Bull. Seism. Soc. Am., 78, pp. 1725-1743.
- Lahr, J. C., (1980), Hypoellipse/Vax: A computer program for determining local earthquake hypocentral parameters, magnitude and first motion pattern, U.S. Geol. Survey Open-File Report 80-59, 67 pp.

Prof. Thomas Ahrens
Seismological Lab, 252-21
Division of Geological & Planetary Sciences
California Institute of Technology
Pasadena, CA 91125

Prof. Keiiti Aki
Center for Earth Sciences
University of Southern California
University Park
Los Angeles, CA 90089-0741

Prof. Shelton Alexander
Geosciences Department
403 Deike Building
The Pennsylvania State University
University Park, PA 16802

Prof. Charles B. Archambeau
CIRES
University of Colorado
Boulder, CO 80309

Dr. Thomas C. Bache, Jr.
Science Applications Int'l Corp.
10260 Campus Point Drive
San Diego, CA 92121 (2 copies)

Prof. Muawia Barazangi
Institute for the Study of the Continent
Cornell University
Ithaca, NY 14853

Dr. Jeff Barker
Department of Geological Sciences
State University of New York
at Binghamton
Vestal, NY 13901

Dr. Douglas R. Baumgardt
ENSCO, Inc
5400 Port Royal Road
Springfield, VA 22151-2388

Dr. Susan Beck
Department of Geosciences
Building #77
University of Arizona
Tucson, AZ 85721

Dr. T.J. Bennett
S-CUBED
A Division of Maxwell Laboratories
11800 Sunrise Valley Drive, Suite 1212
Reston, VA 22091

Dr. Robert Blandford
AFTAC/TT, Center for Seismic Studies
1300 North 17th Street
Suite 1450
Arlington, VA 22209-2308

Dr. Stephen Bratt
ARPA/NMRO
3701 North Fairfax Drive
Arlington, VA 22203-1714

Dr. Lawrence Burdick
IGPP, A-025
Scripps Institute of Oceanography
University of California, San Diego
La Jolla, CA 92093

Dr. Robert Burrige
Schlumberger-Doll Research Center
Old Quarry Road
Ridgefield, CT 06877

Dr. Jerry Carter
Center for Seismic Studies
1300 North 17th Street
Suite 1450
Arlington, VA 22209-2308

Dr. Eric Chael
Division 9241
Sandia Laboratory
Albuquerque, NM 87185

Dr. Martin Chapman
Department of Geological Sciences
Virginia Polytechnical Institute
21044 Derring Hall
Blacksburg, VA 24061

Mr Robert Cockerham
Arms Control & Disarmament Agency
320 21st Street North West
Room 5741
Washington, DC 20451.

Prof. Vernon F. Cormier
Department of Geology & Geophysics
U-45, Room 207
University of Connecticut
Storrs, CT 06268

Prof. Steven Day
Department of Geological Sciences
San Diego State University
San Diego, CA 92182

Marvin Denny
U.S. Department of Energy
Office of Arms Control
Washington, DC 20585

Dr. Cliff Frolich
Institute of Geophysics
8701 North Mopac
Austin, TX 78759

Dr. Zoltan Der
ENSCO, Inc.
5400 Port Royal Road
Springfield, VA 22151-2388

Dr. Holly Given
IGPP, A-025
Scripps Institute of Oceanography
University of California, San Diego
La Jolla, CA 92093

Prof. Adam Dziewonski
Hoffman Laboratory, Harvard University
Dept. of Earth Atmos. & Planetary Sciences
20 Oxford Street
Cambridge, MA 02138

Dr. Jeffrey W. Given
SAIC
10260 Campus Point Drive
San Diego, CA 92121

Prof. John Ebel
Department of Geology & Geophysics
Boston College
Chestnut Hill, MA 02167

Dr. Dale Glover
Defense Intelligence Agency
ATTN: ODT-1B
Washington, DC 20301

Eric Fielding
SNEE Hall
INSTOC
Cornell University
Ithaca, NY 14853

Dan N. Hagedorn
Pacific Northwest Laboratories
Battelle Boulevard
Richland, WA 99352

Dr. Petr Firbas
Institute of Physics of the Earth
Masaryk University Brno
Jecna 29a
612 46 Brno, Czech Republic

Dr. James Hannon
Lawrence Livermore National Laboratory
P.O. Box 808
L-205
Livermore, CA 94550

Dr. Mark D. Fisk
Mission Research Corporation
735 State Street
P.O. Drawer 719
Santa Barbara, CA 93102

Prof. David G. Harkrider
Seismological Laboratory
Division of Geological & Planetary Sciences
California Institute of Technology
Pasadena, CA 91125

Prof Stanley Flatte
Applied Sciences Building
University of California, Santa Cruz
Santa Cruz, CA 95064

Prof. Danny Harvey
CIRES
University of Colorado
Boulder, CO 80309

Prof. Donald Forsyth
Department of Geological Sciences
Brown University
Providence, RI 02912

Prof. Donald V. Helmberger
Seismological Laboratory
Division of Geological & Planetary Sciences
California Institute of Technology
Pasadena, CA 91125

Dr. Art Frankel
U.S. Geological Survey
922 National Center
Reston, VA 22092

Prof. Eugene Herrin
Institute for the Study of Earth and Man
Geophysical Laboratory
Southern Methodist University
Dallas, TX 75275

Prof. Robert B. Herrmann
Department of Earth & Atmospheric Sciences
St. Louis University
St. Louis, MO 63156

Prof. Lane R. Johnson
Seismographic Station
University of California
Berkeley, CA 94720

Prof. Thomas H. Jordan
Department of Earth, Atmospheric &
Planetary Sciences
Massachusetts Institute of Technology
Cambridge, MA 02139

Prof. Alan Kafka
Department of Geology & Geophysics
Boston College
Chestnut Hill, MA 02167

Robert C. Kemerait
ENSCO, Inc.
445 Pineda Court
Melbourne, FL 32940

Dr. Karl Koch
Institute for the Study of Earth and Man
Geophysical Laboratory
Southern Methodist University
Dallas, Tx 75275

Dr. Max Koontz
U.S. Dept. of Energy/DP 5
Forrestal Building
1000 Independence Avenue
Washington, DC 20585

Dr. Richard LaCoss
MIT Lincoln Laboratory, M-200B
P.O. Box 73
Lexington, MA 02173-0073

Dr. Fred K. Lamb
University of Illinois at Urbana-Champaign
Department of Physics
1110 West Green Street
Urbana, IL 61801

Prof. Charles A. Langston
Geosciences Department
403 Deike Building
The Pennsylvania State University
University Park, PA 16802

Jim Lawson, Chief Geophysicist
Oklahoma Geological Survey
Oklahoma Geophysical Observatory
P.O. Box 8
Leonard, OK 74043-0008

Prof. Thorne Lay
Institute of Tectonics
Earth Science Board
University of California, Santa Cruz
Santa Cruz, CA 95064

Dr. William Leith
U.S. Geological Survey
Mail Stop 928
Reston, VA 22092

Mr. James F. Lewkowicz
Phillips Laboratory/GPEH
29 Randolph Road
Hanscom AFB, MA 01731-3010(2 copies)

Mr. Alfred Lieberman
ACDA/VI-OA State Department Building
Room 5726
320-21st Street, NW
Washington, DC 20451

Prof. L. Timothy Long
School of Geophysical Sciences
Georgia Institute of Technology
Atlanta, GA 30332

Dr. Randolph Martin, III
New England Research, Inc.
76 Olcott Drive
White River Junction, VT 05001

Dr. Robert Masse
Denver Federal Building
Box 25046, Mail Stop 967
Denver, CO 80225

Dr. Gary McCartor
Department of Physics
Southern Methodist University
Dallas, TX 75275

Prof. Thomas V. McEvilly
Seismographic Station
University of California
Berkeley, CA 94720

Dr. Art McGarr
U.S. Geological Survey
Mail Stop 977
U.S. Geological Survey
Menlo Park, CA 94025

Dr. Keith L. McLaughlin
S-CUBED
A Division of Maxwell Laboratory
P.O. Box 1620
La Jolla, CA 92038-1620

Stephen Miller & Dr. Alexander Florence
SRI International
333 Ravenswood Avenue
Box AF 116
Menlo Park, CA 94025-3493

Prof. Bernard Minster
IGPP, A-025
Scripps Institute of Oceanography
University of California, San Diego
La Jolla, CA 92093

Prof. Brian J. Mitchell
Department of Earth & Atmospheric Sciences
St. Louis University
St. Louis, MO 63156

Mr. Jack Murphy
S-CUBED
A Division of Maxwell Laboratory
11800 Sunrise Valley Drive, Suite 1212
Reston, VA 22091 (2 Copies)

Dr. Keith K. Nakanishi
Lawrence Livermore National Laboratory
L-025
P.O. Box 808
Livermore, CA 94550

Prof. John A. Orcutt
IGPP, A-025
Scripps Institute of Oceanography
University of California, San Diego
La Jolla, CA 92093

Prof. Jeffrey Park
Kline Geology Laboratory
P.O. Box 6666
New Haven, CT 06511-8130

Dr. Howard Patton
Lawrence Livermore National Laboratory
L-025
P.O. Box 808
Livermore, CA 94550

Dr. Frank Pilotte
HQ AFTAC/TT
1030 South Highway A1A
Patrick AFB, FL 32925-3002

Dr. Jay J. Pulli
Radix Systems, Inc.
201 Perry Parkway
Gaithersburg, MD 20877

Dr. Robert Reinke
ATTN: FCTVTD
Field Command
Defense Nuclear Agency
Kirtland AFB, NM 87115

Prof. Paul G. Richards
Lamont-Doherty Geological Observatory
of Columbia University
Palisades, NY 10964

Mr. Wilmer Rivers
Teledyne Geotech
314 Montgomery Street
Alexandria, VA 22314

Dr. Alan S. Ryall, Jr.
ARPA/NMRO
3701 North Fairfax Drive
Arlington, VA 22203-1714

Dr. Richard Sailor
TASC, Inc.
55 Walkers Brook Drive
Reading, MA 01867

Prof. Charles G. Sammis
Center for Earth Sciences
University of Southern California
University Park
Los Angeles, CA 90089-0741

Prof. Christopher H. Scholz
Lamont-Doherty Geological Observatory
of Columbia University
Palisades, NY 10964

Dr. Susan Schwartz
Institute of Tectonics
1156 High Street
Santa Cruz, CA 95064

Secretary of the Air Force
(SAFRD)
Washington, DC 20330

Office of the Secretary of Defense
DDR&E
Washington, DC 20330

Thomas J. Sereno, Jr.
Science Application Int'l Corp.
10260 Campus Point Drive
San Diego, CA 92121

Dr. Michael Shore
Defense Nuclear Agency/SPSS
6801 Telegraph Road
Alexandria, VA 22310

Dr. Robert Shumway
University of California Davis
Division of Statistics
Davis, CA 95616

Dr. Matthew Sibol
Virginia Tech
Seismological Observatory
4044 Derring Hall
Blacksburg, VA 24061-0420

Prof. David G. Simpson
IRIS, Inc.
1616 North Fort Myer Drive
Suite 1050
Arlington, VA 22209

Donald L. Springer
Lawrence Livermore National Laboratory
L-025
P.O. Box 808
Livermore, CA 94550

Dr. Jeffrey Stevens
S-CUBED
A Division of Maxwell Laboratory
P.O. Box 1620
La Jolla, CA 92038-1620

Lt. Col. Jim Stobie
ATTN: AFOSR/NL
110 Duncan Avenue
Bolling AFB
Washington, DC 20332-0001

Prof. Brian Stump
Institute for the Study of Earth & Man
Geophysical Laboratory
Southern Methodist University
Dallas, TX 75275

Prof. Jeremiah Sullivan
University of Illinois at Urbana-Champaign
Department of Physics
1110 West Green Street
Urbana, IL 61801

Prof. L. Sykes
Lamont-Doherty Geological Observatory
of Columbia University
Palisades, NY 10964

Dr. David Taylor
ENSCO, Inc.
445 Pineda Court
Melbourne, FL 32940

Dr. Steven R. Taylor
Los Alamos National Laboratory
P.O. Box 1663
Mail Stop C335
Los Alamos, NM 87545

Prof. Clifford Thurber
University of Wisconsin-Madison
Department of Geology & Geophysics
1215 West Dayton Street
Madison, WI 53706

Prof. M. Nafi Toksoz
Earth Resources Lab
Massachusetts Institute of Technology
42 Carleton Street
Cambridge, MA 02142

Dr. Larry Turnbull
CIA-OSWR/NED
Washington, DC 20505

Dr. Gregory van der Vink
IRIS, Inc.
1616 North Fort Myer Drive
Suite 1050
Arlington, VA 22209

Dr. Karl Veith
EG&G
5211 Auth Road
Suite 240
Suitland, MD 20746

Prof. Terry C. Wallace
Department of Geosciences
Building #77
University of Arizona
Tuscon, AZ 85721

Dr. Thomas Weaver
Los Alamos National Laboratory
P.O. Box 1663
Mail Stop C335
Los Alamos, NM 87545

Dr. William Wortman
Mission Research Corporation
8560 Cinderbed Road
Suite 700
Newington, VA 22122

Prof. Francis T. Wu
Department of Geological Sciences
State University of New York
at Binghamton
Vestal, NY 13901

Prof Ru-Shan Wu
University of California, Santa Cruz
Earth Sciences Department
Santa Cruz
, CA 95064

ARPA, OASB/Library
3701 North Fairfax Drive
Arlington, VA 22203-1714

HQ DNA
ATTN: Technical Library
Washington, DC 20305

Defense Intelligence Agency
Directorate for Scientific & Technical Intelligence
ATTN: DTIB
Washington, DC 20340-6158

Defense Technical Information Center
Cameron Station
Alexandria, VA 22314 (2 Copies)

TACTEC
Battelle Memorial Institute
505 King Avenue
Columbus, OH 43201 (Final Report)

Phillips Laboratory
ATTN: XPG
29 Randolph Road
Hanscom AFB, MA 01731-3010

Phillips Laboratory
ATTN: GPE
29 Randolph Road
Hanscom AFB, MA 01731-3010

Phillips Laboratory
ATTN: TSML
5 Wright Street
Hanscom AFB, MA 01731-3004

Phillips Laboratory
ATTN: PL/SUL
3550 Aberdeen Ave SE
Kirtland, NM 87117-5776 (2 copies)

Dr. Michel Bouchon
I.R.I.G.M.-B.P. 68
38402 St. Martin D'Heres
Cedex, FRANCE

Dr. Michel Campillo
Observatoire de Grenoble
I.R.I.G.M.-B.P. 53
38041 Grenoble, FRANCE

Dr. Kin Yip Chun
Geophysics Division
Physics Department
University of Toronto
Ontario, CANADA

Prof. Hans-Peter Harjes
Institute for Geophysics
Ruhr University/Bochum
P.O. Box 102148
4630 Bochum 1, GERMANY

Prof. Eystein Husebye
NTNF/NORSAR
P.O. Box 51
N-2007 Kjeller, NORWAY

David Jepsen
Acting Head, Nuclear Monitoring Section
Bureau of Mineral Resources
Geology and Geophysics
G.P.O. Box 378, Canberra, AUSTRALIA

Ms. Eva Johannisson
Senior Research Officer
FOA
S-172 90 Sundbyberg, SWEDEN

Dr. Peter Marshall
Procurement Executive
Ministry of Defense
Blacknest, Brimpton
Reading FG7-FRS, UNITED KINGDOM

Dr. Bernard Massinon, Dr. Pierre Mechler
Societe Radiomana
27 rue Claude Bernard
75005 Paris, FRANCE (2 Copies)

Dr. Svein Mykkeltveit
NTNT/NORSAR
P.O. Box 51
N-2007 Kjeller, NORWAY (3 Copies)

Prof. Keith Priestley
University of Cambridge
Bullard Labs, Dept. of Earth Sciences
Madingley Rise, Madingley Road
Cambridge CB3 0EZ, ENGLAND

Dr. Jorg Schlittenhardt
Federal Institute for Geosciences & Nat'l Res.
Postfach 510153
D-30631 Hannover, GERMANY

Dr. Johannes Schweitzer
Institute of Geophysics
Ruhr University/Bochum
P.O. Box 1102148
4360 Bochum 1, GERMANY

Trust & Verify
VERTIC
Carrara House
20 Embankment Place
London WC2N 6NN, ENGLAND